UNIVERSIDADE
BEIRA INTERIOR

Carbon felt-based electrochemical processes in the treatment of winery wastewater

(Versão final após defesa)

Pedro José Ferreira Gonçalves

Dissertação para obtenção do Grau de Mestre em
Química Industrial
(2º ciclo de estudos ou mestrado integrado)

Orientador: Prof.ª Doutora Ana Maria Carreira Lopes
Co-orientador: Doutora Annabel Dias Barrocas Fernandes

janeiro de 2024

Declaração de Integridade

Eu, Pedro José Ferreira Gonçalves, que abaixo assino, estudante com o número de inscrição M10749 de Química Industrial da Faculdade de Ciências, declaro ter desenvolvido o presente trabalho e elaborado o presente texto em total consonância com o **Código de Integridades da Universidade da Beira Interior**.

Mais concretamente afirmo não ter incorrido em qualquer das variedades de Fraude Académica, e que aqui declaro conhecer, que em particular atendi à exigida referenciação de frases, extratos, imagens e outras formas de trabalho intelectual, e assumindo assim na íntegra as responsabilidades da autoria.

Universidade da Beira Interior, Covilhã 23 /01 /2024

Resumo

A indústria vinícola produz grandes quantidades de efluente, com elevada carga orgânica, que tem de ser tratado antes de ser descarregado nos meios aquáticos naturais ou reutilizado. Para este fim, os processos eletroquímicos são uma alternativa inovadora comparativamente aos processos biológicos tradicionais, sendo assim o foco deste trabalho.

O tratamento eletroquímico de efluentes é já vastamente estudado, pelo que este trabalho incide no estudo de um novo material no tratamento de efluente vinícola, o carbon felt, e o seu potencial como material de elétrodo em dois processos eletroquímicos, o eletro-Fenton e a oxidação eletroquímica.

Foram estabelecidos múltiplos ensaios, tendo o carbon felt sido usado como ânodo e como cátodo, e tendo sido avaliadas a sua eficiência, reprodutibilidade e durabilidade. Outros parâmetros, como a intensidade de corrente e a possível adição de eletrólitos, também foram estudados.

Os resultados mostraram que o carbon felt tem potencial para ser utilizado em processos eletroquímicos, pois obteve resultados semelhantes aos de outros materiais já bastante utilizados, como o diamante dopado com boro, quando utilizado como ânodo, e como o aço inoxidável, quando usado como cátodo. A sua reprodutibilidade também demonstrou resultados positivos. No entanto, a sua durabilidade não é a melhor, o que pode levar a futuros estudos para o melhoramento da sua durabilidade, bem como para a otimização do processo.

Palavras-chave

Efluente vinícola; Eletro-Fenton; Oxidação eletroquímica; Carbon felt

Abstract

The wine industry produces large amounts of wastewater, with this normally having a high organic load, and thus requiring treatment before discharge in the natural water courses. For this purpose, the electrochemical processes are an innovative alternative to the traditional biological processes, and as so, they are the focus of this work.

Electrochemical treatment of wastewaters is already widely researched, so this work focused on studying a novel material in the treatment of winery wastewater, the carbon felt, and its potential as electrode material in two electrochemical processes, the electro-Fenton and the electrochemical oxidation.

Multiple experiments were setup, and carbon felt was used both as an anode and as a cathode, and its process efficiency, reproducibility and durability were evaluated. Other parameters like current intensity and possible addition of electrolytes were also assessed.

Results have shown that carbon felt as the potential of being used in electrochemical processes, having obtained similar load removal rates as some widely used materials, like boron-doped diamond, when used as an anode, and stainless steel, when used as a cathode. Its reproducibility also demonstrated positive results. However, its durability is somewhat lacking which could incite future studies towards the improvement of its durability and optimization of the process.

Keywords

Winery wastewater; Electro-Fenton; Electrochemical oxidation; Carbon felt

Index

Resumo v
Abstract vii
Index ix
Figure index xi
Table index xiii
Abbreviation list xv
Chapter 1 1
1.1 Environmental context 1
1.2 Global aims and strategy 1
1.3 Thesis overview 2
Chapter 2 - Electrochemical technologies in winery wastewater treatment - Fundamentals and literature review 3
2.1 Electro-Fenton 3
2.2 Electrochemical oxidation 9
Chapter 3 – Materials and methods 17
3.1 Winery wastewater 17
3.2 Electrochemical degradation study 17
3.2.1 Electro-Fenton experiments 18
3.2.2 Electrochemical oxidation experiments 19
3.3 Analytical methods 21
3.3.1 Chemical oxygen demand 22
3.3.2 Total, organic, and inorganic carbon 23
3.3.3 Total nitrogen 23
3.3.4 pH 24
3.3.5 Electrical conductivity 24
3.3.6 Total dissolved iron and dissolved iron(II) 24
3.3.7 Hydrogen peroxyde 25
3.3.9 Scanning electron microscopy 26
Chapter 4 – Results and Discussion 27
4.1 Electro-Fenton experiments 27
4.2 Electrochemical oxidation experiments 30
Chapter 5 – Conclusions and future perspectives 43
References 45

Figure index

2.1 Schematic diagram of an EF cell with the main reactions involved when a carbonaceous material cathode is used (Fernandes et al., 2015).

3.1 Schematic representation of the experimental setup utilized in the electro-Fenton experiments.

3.2 Schematic representation of the experimental setup utilized in the electro-oxidation experiments.

3.3 Linear relationship between absorbance at 511 nm and the concentration of a) Fe^{2+} and b) TDI.

3.4 Linear relationship between absorbance at 450 nm and the concentration of H_2O_2.

4.1 Relative variation of (a) COD, (b) TC, and (c) TOC with time for the EF assays performed with winery wastewater.

4.2 Variation of (a) Fe^{2+} concentration, (b) Fe_{total} concentration, (c) H_2O_2 concentration, and (d) pH with time for the EF assays performed on winery wastewater.

4.3 Variation of (a) conductivity, and (b) potential with time for the EF assays performed on winery wastewater.

4.4 Experimental results of EO assays with a BDD anode: Variation of (a) COD, (c) TOC, and (e) IC with time for experiments at 0.1 A; Variation of (b) COD, (d) TOC, and (f) IC with time for experiments at 0.5 A.

4.5 Experimental results of EO assays with a BDD anode: Variation of a) pH; c) conductivity with time for experiments with 0.1 A; Variation of b) pH; d) conductivity with time for experiments with 0.5 A.

4.6 Variation with time of different parameters during EO assays with a carbon felt anode: a) COD; b) TOC; c) IC; d) TC; e) pH; f) conductivity.

4.7 Experimental results for the EO assays performed with different electrode combinations and applied current intensity: a) COD; b) TOC; c) TC; d) IC.

4.8 Experimental results for EO assays run with different electrode combinations and applied current intensity: a) pH; b) conductivity.

4.9 SEM results of the analysis of the CF anode in the assay with a SS cathode: a) before the assay - 100x amplification; b) before the assay - 5000x amplification; c) after the assay - 100x amplification; d) after the assay - 5000x amplification.

4.10 Variation of COD with time for the experiments run at (a) continuous polarity, and (b) polarity reversal.

4.11 Variation of TC with time for the assays performed at (a) continuous polarity, and (b) polarity reversal.

4.12 Variation of IC with time for the assays performed at (a) continuous polarity, and (b) polarity reversal.

4.13 Variation of TOC with time for the assays performed at (a) continuous polarity, and (b) polarity reversal.

4.14 Variation of pH with time for the assays performed at (a) continuous polarity, and (b) polarity reversal.

4.15 Variation of conductivity with time for the assays performed at (a) continuous polarity, and (b) polarity reversal.

4.16 SEM results of the analysis of the CF anode in the assays run at continuous polarity: top row - 100x amplification; bottom row - 5000x amplification.

4.17 SEM results of the analysis of the CF cathode in the assays run at continuous polarity: top row - 100x amplification; bottom row - 5000x amplification.

4.18 SEM results of the analysis of the CF anode in the assays run with polarity reversal: top row - 100x amplification; bottom row - 5000x amplification.

4.19 SEM results of the analysis of the CF cathode in the assays run with polarity reversal: top row - 100x amplification; bottom row - 5000x amplification.

4.20 Variation of COD, TC, IC, and TOC during each cycle.

4.21 SEM results of the analysis of the CF anode used at the consecutive assays of 24-h duration: top row - 100x amplification; bottom row - 5000x amplification.

4.22 SEM results of the analysis of the CF cathode used at the consecutive assays of 24-h duration: top row - 100x amplification; bottom row - 5000x amplification.

Table index

2.1 A summary of the research results previously reported for the degradation of winery wastewater by electro-Fenton.

2.2 A summary of the research results previously reported for the degradation of winery wastewater by electrochemical oxidation.

3.1 Characterization of the winery wastewater used in the electrochemical study, before and after being spiked with commercial wine.

3.2 Description of the different experimental variables' combination studied for EF process.

3.3 Description of the different experimental variables' combination studied in the first group of EO experiments.

3.4 Description of the different experimental variables' combination studied in the second group of EO experiments.

Abbreviation list

A	Electrode area
Abs	Absorbance
AO-H_2O_2	Anodic oxidation with electrogenerated H_2O_2
BDD	Boron-doped diamond
C	Concentration
CF	Carbon felt
COD	Chemical oxygen demand
COD_0	Chemical oxygen demand before electrolysis
COD_{cr}	Critical chemical oxygen demand
COD(t)	Chemical oxygen demand at electrolysis time t
EC	Electrical conductivity
EF	Electro-Fenton
EO	Electrochemical oxidation
F	Faraday constant
I	Applied current intensity
IC	Inorganic carbon
ICE	Instantaneous current efficiency
j	Current density
j_{lim}	Limiting current density
j_{lim_0}	Initial limiting current density
k_m	Mass transport coefficient
NDIR	Non-dispersive infrared detector
PEF	UVA photoelectro-Fenton
SEM	Scanning electron microscopy
SPEF	Solar photoelectro-Fenton
t	Electrolysis time
TC	Total carbon
t_{cr}	Critical time
TDI	Total dissolved iron
TN	Total nitrogen
TOC	Total organic carbon
V	Volume

WW	Winery wastewater
α	Ratio between current density and initial limiting current density

Chapter 1

An overview of the reasons for creating this work is provided in this chapter. Additionally, it specifies the goals set forward and the plan used to achieve them. At the end of the chapter, a summary of this thesis's content is presented.

1.1 Environmental context

Large amounts of water are used in the industrial production of wine, with about 70% of that water being released as wastewater. Winery wastewater (WW) is typically characterized by high salinity and organic load with a wide variety of organic molecules, including organic acids, sugars, alcohols, and recalcitrant high-molecular weight compounds. This highly polluted WW should not be disposed of in water courses since it will impact ecosystems and water quality (Davididou & Frontistis, 2021).

One of the main issues with winery wastewater is the presence of hazardous and resistant chemicals that are very difficult to breakdown through standard biological treatment processes (Ippolito et al., 2021). Phenolic compounds, which are found in the stems, seeds, and skins of grapes and are formed during the winemaking process, are the most prevalent recalcitrant and hazardous substances that can be detected in WW. These compounds are the ones mainly responsible for the color and toxicity of winery wastewater. Their resistance to biological degradation and subsequent persistence in the treated WW are of great concern (Strong & Burgess, 2008).

The ability of wastewater treatment plants to carry out efficient winery wastewater treatment is affected by the presence of recalcitrant compounds as well as high WW variability (Johnson & Mehrvar, 2020). Electrochemical processes emerge as a new option to treat WW while pairing it with the traditional biological treatments or substituting them altogether. The use of electrochemical processes in winery wastewaters is described, with encouraging outcomes, in several articles, being these further analyzed later in this thesis.

1.2 Global aims and strategy

The main goal of this work was to study the efficiency of carbon felt (CF) as electrode material in the treatment of winery wastewater through electrochemical processes.

With this purpose and considering the already established boron-doped diamond (BDD) anode as a standard in electrochemical processes, the following secondary goals were established:

1. Study the process efficiency of two electrochemical processes in the treatment of WW, namely electro-Fenton (EF) and electrochemical oxidation (EO).

2. Compare the results obtained with a carbon felt anode to those of a standard BDD anode.

3. Study other process variables and their influence in the efficiency of the process.

4. Evaluate the durability and reproducibility of CF electrodes during these processes.

To achieve the goals proposed, several sets of experiments were performed at different operational conditions, with experiments being divided in two sets, a first one that focused on the EF process, where it was only studied a combination of a BDD anode and a CF cathode, something not yet reported in literature.

In the second set of experiments, the EO process was the focus, and here the carbon felt was studied as competing anode material to BDD. Repetitive assays and consecutive experiments were also performed to evaluate the durability and reproducibility of this material.

1.3 Thesis overview

This thesis is structured in five main chapters. In the first and present chapter, the motivations to perform this work and its environmental background are presented. The global aims of the work are listed, and the plan used to achieve them is described.

The second chapter follows as a concise literature review on the fundamentals and applications of the electrochemical processes studied in this work, namely electro-Fenton, and electrochemical oxidation. Their application in winery wastewater treatment is further described deeply.

Subsequently, the third chapter presents the characterization of the winery wastewater samples used in this work and the description of the electrochemical experiments and of the analytical methods used to evaluate those experiments.

Chapter four presents the results obtained in the different experiments performed as described in the third chapter. The results are here discussed, and the main conclusions are presented.

Finally, the fifth chapter summarizes the results and conclusions obtained during this research study, regarding the application and optimization of electrochemical processes in winery wastewater treatment. Future perspectives are also discussed.

Chapter 2 - Electrochemical technologies in winery wastewater treatment - Fundamentals and literature review

2.1 Electro-Fenton

The electro-Fenton processes are derived from the Fenton reaction, a reaction based on an electron transfer between H_2O_2 and Fe^{2+}, which was first observed by Fenton in 1984. This reaction produces hydroxyl radical (Equation 2.1), which is a very strong oxidizing species (Deng et al., 2006).

$$Fe^{2+}\ (aq) + H_2O_2\ (l) \rightarrow Fe^{3+}\ (aq) + HO^{\bullet}\ (aq) + OH^{-}\ (aq) \quad (2.1)$$

Once formed, hydroxyl radicals attack almost all organic molecules. Depending on the nature of the organic species, two kinds of initial attack are possible: the hydroxyl radical can abstract a hydrogen atom to form water (Equation 2.2), in the case of alkanes or other saturated molecules, or it can add to the contaminant, as is the case for alkenes, aromatic compounds or other unsaturated molecules (Equation 2.3). In the presence of oxygen, the attack by the hydroxyl radical initiates a complex sequence of oxidative reactions leading to complete mineralization, as it is shown in Equations 2.4–2.7, for alkanes and other saturated molecules, and in Equations 2.8–2.9, for alkenes, aromatic compounds, and other unsaturated molecules, where R, R_1 and R_2 represent an organic chain of any length (Solarchem Environmental Systems, 1994).

$$RCH_3\ (aq) + HO^{\bullet}\ (aq) \rightarrow RC^{\bullet}H_2\ (aq) + H_2O\ (l) \quad (2.2)$$

$$R_1{=}R_2\ (aq) + HO^{\bullet}\ (aq) \rightarrow HOR_1\text{-}R_2^{\bullet}\ (aq) \quad (2.3)$$

$$RC^{\bullet}H_2\ (aq) + HO^{\bullet}\ (aq) \rightarrow RCH_2OH\ (aq) \quad (2.4)$$

$$RCH_2OH\ (aq) + 2\ HO^{\bullet}\ (aq) \rightarrow RHC{=}O\ (aq) + 2\ H_2O\ (l) \quad (2.5)$$

$$RHC{=}O\ (aq) + 2\ HO^{\bullet}\ (aq) \rightarrow RCOOH\ (aq) + H_2O\ (l) \quad (2.6)$$

$$RCOOH\ (aq) + 2\ HO^{\bullet}\ (aq) \rightarrow CO_2\ (aq) + ROH \quad (2.7)$$

$$HOR_1\text{-}R_2^{\bullet}\ (aq) + HO^{\bullet}\ (aq) \rightarrow HOR_1\text{-}R_2OH\ (aq) \quad (2.8)$$

$$HOR_1\text{-}R_2OH\ (aq) + 2\ HO^{\bullet}\ (aq) \rightarrow R_1{=}O\ (aq) + R_2{=}O\ (aq) + 2\ H_2O\ (l) \quad (2.9)$$

In the conventional wastewater treatment processes involving the Fenton reaction, the Fenton reagents (H_2O_2 and an Fe(II) salt) are added to the target wastewater to be treated, which in itself is an inconvenience, since H_2O_2 is a reactive reagent and is unsafe to transport, store, and handle. Besides that, there is also a problem with the formation of Fe^{3+} during the Fenton process because Fe^{3+} precipitates in the form of iron oxyhydroxides, especially at high pH, resulting in the production of iron sludge, which must be treated and disposed of properly (Umar et al., 2010; Wang et al., 2012). The emergence of the electro-Fenton process, an electrochemical oxidation method based on the Fenton reaction, was a step forward in trying to overcome these drawbacks.

In the EF process, an indirect electrochemical oxidation of the organic compounds occurs through hydroxyl radicals, generated by the Fenton reaction, with both H_2O_2 and Fe^{2+} being possibly electrogenerated *in situ* (Deng et al., 2006). These processes can be operated through many different configurations: Fe^{2+} is externally added, with both H_2O_2 and Fe^{2+} being concurrently generated/regenerated at the cathode; H_2O_2 is externally supplied, while a sacrificial iron anode is used as Fe^{2+} source; H_2O_2 is externally added and Fe^{2+} is electrogenerated via reduction of Fe^{3+}; both Fe^{2+} and H_2O_2 are electrogenerated at a sacrificial iron anode and at the cathode, respectively (Orkun et al., 2012).

The electrogeneration of H_2O_2 at the cathode, via Equation 2.10, is made possible when the cathode is made of carbonaceous materials or noble metal alloys, with O_2 being either fed into the reactor or directly electrogenerated in the presence of noble metal anodes, as described in the literature (Wang et al., 2012; Perry et al., 2019). In the presence of ferrous ions, hydroxyl radicals may be formed (Eq. 2.1), while producing ferric ions. The strong oxidant hydroxyl radical, thus formed, is capable of oxidize the organic matter (Fig. 2.1). Besides being a product of the Fenton reaction, hydroxyl radical can also be produced at the surface of a high-oxygen overvoltage anode, from water oxidation via Equation 2.11 (Zhang et al., 2006). Due to the continuous regeneration of Fe^{2+} at the cathode, via Eq. 2.12, the production of hydroxyl radical (Eq. 2.1) can be increased, and the iron sludge production minimized (Sirés et al., 2007; Zhang et al., 2012). Nonetheless, the increase in ferrous ions can decrease the process efficiency through Eq. 2.13 (Fernandes et al., 2017). These reactions can be illustrated in the context of an EF process by Figure 2.1.

$$O_2\ (g) + 2\ H^+\ (aq) + 2\ e^- \rightarrow H_2O_2\ (l) \quad (2.10)$$

$$H_2O\ (l) \rightarrow HO^{\bullet}\ (aq) + H^+\ (aq) + e^- \quad (2.11)$$

$$Fe^{3+}\ (aq) + e^- \rightarrow Fe^{2+}\ (aq) \quad (2.12)$$

$$Fe^{2+}\ (aq) + HO^{\bullet}\ (aq) \rightarrow Fe^{3+}\ (aq)\ + OH^-\ (aq) \quad (2.13)$$

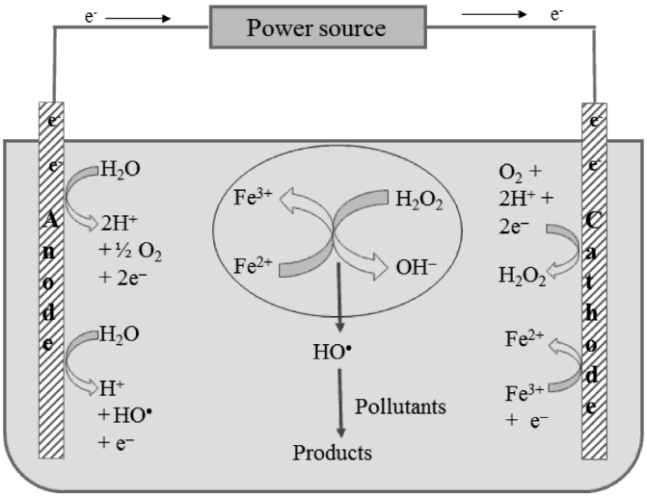

Figure 2.1 – Schematic diagram of an EF cell with the main reactions involved when a carbonaceous material cathode is used (Fernandes et al., 2015).

The selection of anode and cathode materials is an important aspect in the EF process. If it is not aimed to electrogenerate Fe^{2+} through a sacrificial iron anode, the anode should be made of a stable material, which do not deteriorate in the electrolytic cells, and present a high-oxygen overvoltage, so it can efficiently produce hydroxyl radicals in the EF process (Nidheesh & Gandhimathi, 2012). For a long time, Pt was one of the most used anode materials in EF process, due to its good conductivity and chemical stability, even at high potentials and in very corrosive media (Nidheesh & Gandhimathi, 2012). Nevertheless, Pt anodes are expensive and present low mineralization yield, which precludes their industrial application. Still, they continue to be widely used for small-scale oxidation processes in laboratory studies (Santos et al., 2022). Boron-doped diamond anodes are currently the most applied in electrooxidation processes, due to their extraordinary properties. These include inert surface with low adsorption properties, outstanding corrosion stability even in strongly acidic media and extremely high O_2 evolution overvoltage, which results in enhanced electrogeneration of $HO^{\bullet}$ radicals and, consequently, boosts the oxidation mechanism of EF processes. Although BDD is also an expensive material, its high durability and stability helps to balance its high cost (Santos et al., 2022). Regarding the cathode material, if the electrogeneration of H_2O_2 is desired, it is required that it has a good catalytic activity for oxygen reduction, as this contributes to high H_2O_2 electrogeneration (Eq. 2.10). There are several materials being used, ranging from metals like stainless steel, to metal oxides, and composites on supporting carbonaceous materials such as graphene or carbon felt (Fernandes et al., 2015; Santos et al., 2022).

Electro-Fenton processes have been used in the degradation of a broad range of wastewaters, like textile (Karimi et al., 2022), tannery (Doumbi et al., 2022), sanitary landfill leachate (Fernandes et al., 2016, 2017, 2019), olive mill (Ltaïef et al., 2019), or

brewing leachate (Yang et al., 2022), and some specific target compounds, like micropollutants (Chen et al., 2022) or hydrophilic organic pollutants (Zhang et al., 2022). Nevertheless, there are few applications of this method for winery wastewater treatment.

Table 2.1 shows a compilation of the major studies performed, with a summary of the main experimental conditions used and results obtained. In all these studies with WW, the configuration used for the EF process was the one where iron is externally added into the wastewater, while H_2O_2 is electrogenerated *in situ*, via O_2 from air fed near the cathode (Eq. 2.10). Moreira et al. (2015) and Diez et al. (2016) used carbonaceous cathodes, which have shown good efficiencies for H_2O_2 generation, whereas Iglesias et al. (2015) used a nickel foam cathode, which, besides having a higher reaction surface, is also able to produce an additional H_2O_2 amount via superoxide radical. As for the anode material, BDD was the most studied.

Fenton reagents (H_2O_2 and an Fe(II) salt) concentration is one of the key operational parameters that affects the efficiency of EF processes and it should be optimized, to obtain the maximum mineralization in the process (Fernandes et al., 2015).

Although none of reported studies tried to add H_2O_2 or vary its concentration, the effect of the iron concentration on the performance of EF processes was studied in the works of Iglesias et al. (2015) and Moreira et al. (2015). It was concluded that a progressively faster mineralization can be obtained at higher Fe^{2+} concentrations, but, if there is too much iron content introduced, a negative effect will occur on the degradation of organic matter, because an excess on Fe^{2+} on the media consumes $HO^{\bullet}$ (Eq. 2.13), while the produced Fe^{3+} would consume H_2O_2 (Eq. 2.14) (Iglesias et al., 2015; Moreira et al., 2015).

$$Fe^{3+}\,(aq) + H_2O_2\,(l) \rightarrow Fe^{2+}\,(aq) + HO_2^{\bullet}\,(aq) + H^{+}\,(aq) \quad (2.14)$$

The winery wastewater utilized in the study performed by Iglesias et al. (2015) presented the highest chemical oxygen demand (COD) value of all the studies found, with 52.8 g L^{-1}. For this, heterogeneous electro-Fenton experiments were carried out using 150 mL of WW with different supporting catalysts as iron source. The effect of the applied potential on COD and color removal was investigated by varying the applied voltage between 5 and 15 V. It was found that COD removal and discoloration rate increased with the applied potential (Table 2.1). The increase in the applied potential increases H_2O_2 production and, consequently, $HO^{\bullet}$ formation, resulting in more oxidizing species to react with pollutant molecules (Iglesias et al., 2015).

Table 2.1 – A summary of the research results previously reported for the degradation of winery wastewater by electro-Fenton.

Anode / cathode	Inter-electrode gap / cm	COD_0 / mg L^{-1}	[Fe] / mg L^{-1}	pH_0	Applied current density / Potential	Operation time / h	COD,TOC,color removal / %	References
BDD / nickel foam	6	52800	40.2[a] (Fe^{2+})	3.2	15 V	24	82 (COD)	Iglesias et al. (2015)
					10 V		79 (COD)	
					5 V		71 (COD)	
BDD / carbon-PTFE	0.5	380	35 (Fe^{2+})	2.8	25 mA cm^{-2}	4	54 (TOC)	Moreira et al. (2015)
Graphite / graphite	8	14430	75 (Fe^{3+})	2	5 V	5.67	66 (color)	Diez et al. (2016)

[a] Value obtained indirectly from data presented in the reference.

Moreira et al. (2015) implemented a dual oxidation process, combining EF with aerobic biological oxidation, with the latter one mineralizing the biodegradable fraction of the wastewater, whereas EF mineralize the recalcitrant fraction afterwards. The WW used in this work had a COD of 12 g L^{-1}, with 97% being removed in the biological oxidation step, leaving 380 mg L^{-1} to be treated by EF process, which resulted in a removal of total organic carbon (TOC) of 54%. In addition to the EF process, there were three other similar electrochemical advanced oxidation processes studied, namely, anodic oxidation with electrogenerated H_2O_2 (AO-H_2O_2), UVA photoelectro-Fenton (PEF) and solar PEF (SPEF). The results demonstrated that the relative oxidative ability of these processes increased in the order AO-H_2O_2 < EF < PEF ≤ SPEF, with PEF and SPEF processes reaching 84 and 86% TOC removal, respectively. This shows that the EF process can still be further optimized beyond its conventional operational method.

Diez et al. (2016) also studied different processes based on the Fenton reaction and their ability to mineralize a winery wastewater. In this work, electrochemical degradation, EF and PEF were evaluated with results showing that PEF process was the most effective, reaching a discoloration of 71%. The PEF process was then further optimized, until discoloration levels of 97% were reached. This work was followed up by two additional studies, focusing only on the PEF process (Diez et al., 2017a, 2017b).

2.2. Electrochemical oxidation

The most widely used electrochemical method for eliminating organic contaminants from wastewaters is electrochemical oxidation (Martínez-Huitle & Brillas, 2009). It is an electrolysis-based process that, in its most basic form, involves oxidizing contaminants in an electrolytic cell made up of two electrodes coupled by an external circuit so that electrochemical reactions can occur. The species in solution and pollutants can be oxidized by direct anodic oxidation and/or by chemical reaction with electrogenerated species at the anode, such as physically adsorbed "active oxygen" (like the hydroxyl radical) or chemically adsorbed "active oxygen" (oxygen in the lattice of a metal oxide anode) generated from water discharge (Martínez-Huitle & Brillas, 2009; Chiang et al., 1995). To explain this behavior, Comninellis (1994) proposed a model for the oxidation of organic compounds by hydroxyl radicals based on the existence of two types of anodes, the “active” and the “non-active” ones. The suggested model states that there is an initial reaction, common for both types of anodes (generically denoted as M), which corresponds to the oxidation of water molecules to physically adsorbed hydroxyl radical (Eq. 2.15).

$$M + H_2O\,(l) \rightarrow M(^{\bullet}OH) + H^+\,(aq) + e^- \quad (2.15)$$

For “active” anodes, there will be a strong interaction between the anode surface and HO$^{\bullet}$ that will result in the formation of a superoxide (MO), according to Equation 2.16.

$$M(^{\bullet}OH) \rightarrow MO + H^+\,(aq) + e^- \quad (2.16)$$

The redox couple MO/M will serve as a mediator in the oxidation of organic substances (Eq. 2.17), which competes with the side reaction of oxygen evolution from chemically breaking down superoxide (Eq. 2.18).

$$MO + R\,(aq) \rightarrow M + RO \quad (2.17)$$

$$MO \rightarrow M + \tfrac{1}{2}\,O_2\,(g) \quad (2.18)$$

When using "non-active" anodes, interactions between the anode surface and HO$^{\bullet}$ will be so weak that they will permit fully oxidized reaction products, such as CO_2, to be produced directly by organic compounds reacting with M($^{\bullet}$OH) through Equation 2.19, where R is an organic compound with m carbon atoms and no heteroatoms, which needs $a = (2m + n)$ oxygen atoms to be completely mineralized to CO_2. The reactivity for the oxidation of organic molecules increases with a weaker interaction between the anode surface and HO$^{\bullet}$,

resulting in a faster chemical reaction. The side reactions of M(•OH), such as direct oxidation to O_2 (Eq. 2.20) and indirect consumption through dimerization to hydrogen peroxide (Eq. 2.21), will compete with this process (Martínez-Huitle & Brillas, 2009).

$$a\ M(^{\bullet}OH) + R\ (aq) \rightarrow a\ M + m\ CO_2\ (g) + n\ H_2O\ (l) + (a\text{-}2n)\ H^+\ (aq) + (a\text{-}2n)\ e^- \quad (2.19)$$

$$M(^{\bullet}OH) \rightarrow M + \tfrac{1}{2}\ O_2\ (g) + H^+\ (aq) + e^- \quad (2.20)$$

$$2\ M(^{\bullet}OH) \rightarrow 2\ M + H_2O_2\ (l) \quad (2.21)$$

A few examples of “active” anodes are Pt, IrO_2 and RuO_2. While the "non-active" anodes include PbO_2, SnO_2, and BDD. When reactants and/or products from the aqueous media are adsorbed onto a "non-active" anode, there is no catalytic active site available. In this instance, the anode just functions as an inert substrate that can remove electrons (Martínez-Huitle & Brillas, 2009).

Although the Comninellis model (Comninellis, 1994) implies that EO is mediated by hydroxyl radicals, either adsorbed at the surface, in the case of “active” anodes, or just weakly adsorbed, in the case of the “non-active” ones, there are additional oxidizing species that may also be formed by oxidation at the anode, such as ozone, created from water discharge at the anode, H_2O_2, from Equation 2.21, Cl_2, HClO and ClO^-, derivate from Cl^- oxidation at the anode (Eqs. 2.22–2.24), and peroxodisulphate (Eq. 2.25), peroxodicarbonate (Eq. 2.26) and peroxodiphosphate (Eq. 2.27), from the anodic oxidation of bisulphate (or sulphate), bicarbonate and phosphate, respectively (Martínez-Huitle & Brillas, 2009; Martínez-Huitle & Ferro, 2006).

$$Cl^-\ (aq) \rightarrow \tfrac{1}{2}\ Cl_2\ (g) + e^- \quad (2.22)$$

$$Cl_2\ (aq) + H_2O\ (l) \rightarrow HOCl\ (aq) + H^+\ (aq) + Cl^-\ (aq) \quad (2.23)$$

$$HOCl\ (aq) \rightarrow OCl^-\ (aq) + H^+\ (aq) \quad (2.24)$$

$$2\ HSO_4^-\ (aq) \rightarrow S_2O_8^{2-}\ (aq) + 2\ H^+\ (aq) + 2\ e^- \quad (2.25)$$

$$2\ HCO_3^-\ (aq) \rightarrow C_2O_6^{2-}\ (aq) + 2\ H^+\ (aq) + 2\ e^- \quad (2.26)$$

$$2\ PO_4^{3-}\ (aq) \rightarrow P_2O_8^{4-}\ (aq) + 2\ e^- \quad (2.27)$$

Two different oxidation mechanisms may occur during the electrochemical oxidation of an aqueous effluent: (I) electrochemical conversion, in which organic compounds are partially oxidized and changed into a variety of more biodegradable reaction by-products; (II) electrochemical combustion, in which organic compounds are completely mineralized and

transformed into water, carbon dioxide, and other inorganic species, with no further treatment required (Deng et al., 2006, Anglada et al., 2009, Martínez-Huitle & Ferro, 2006).

The EO process selectivity and effectiveness are highly influenced by the anode material. As a result, its choice must be carefully considered. The oxygen evolution overpotential of the anode material can be used to examine the competition between organic compounds oxidation at the anode and the oxygen evolution side reaction. Low O_2 overvoltage anodes will exhibit high oxygen evolution electrochemical activity and low organic compounds oxidation chemical reactivity. At high current densities, oxygen production will cause a significant reduction in current efficiency; consequently, effective oxidation of pollutants at these anodes should occur at low current densities. On the other hand, because higher current densities can be applied with minimal oxygen evolution side reaction contributions at high O_2 overvoltage anodes, these are typically the ones chosen for the EO process (Martínez-Huitle & Brillas, 2009). BDD electrodes have shown to produce the highest organic oxidation rates and current efficiencies among the most frequently utilized anodes in EO (Anglada et al., 2009). In fact, this anode material possesses remarkable characteristics, like an inert surface with low adsorption properties, remarkable corrosion stability even in media with high acidity, and extremely high O_2 evolution overvoltage (Fryda et al., 1999; Panizza et al., 2005).

Panizza et al. (2001) created a theoretical model to forecast the COD and instantaneous current efficiency (ICE) during the electrochemical oxidation of organic pollutants on BDD electrodes in a batch recirculation system under galvanostatic conditions. According to this model, the electrochemical mineralization of organic compounds, which uses electrogenerated $HO^{\bullet}$ radicals and/or direct electron transfer, is a fast process regulated by mass transport of the organic compounds towards the anode. Equation 2.28 may be used to calculate the limiting current density for the electrochemical combustion of organic pollutants under these conditions (Panizza et al., 2001), where j_{lim} is the limiting current density, in A m^{-2}, F is the Faraday constant, in C mol^{-1}, k_m is the mass transport coefficient in the electrochemical reactor, in m s^{-1}, and COD is the chemical oxygen demand, in mol O_2 m^{-3}.

$$j_{lim} = 4 F k_m COD \quad (2.28)$$

Two distinct operating regimes may be identified based on the applied current density (Panizza et al., 2001):

- $j < j_{lim}$

The COD decreases linearly with time, the electrolysis is controlled by the current, and the current efficiency is 100%. Under these conditions, Equation 2.29 can be used to represent the temporal evolution of COD, where COD(t) is the COD at electrolysis time t, in mol O_2 m^{-3}, COD_0 is the COD before electrolysis, in mol O_2 m^{-3}, $\alpha = j/j_{lim_0}$, being j the current density and j_{lim_0} the initial limiting current density, A is the electrode area, in m^2, V is the sample volume, in m^3, and t is the electrolysis time, in s.

$$COD(t) = COD_0 \left(1 - \frac{\propto A\, k_m}{V}\, t\right) \quad (2.29)$$

Replacing j by I/A, where I is the applied current intensity, in A, and j_{lim_0} by ($4\, F\, k_m\, COD_0$), Equation 2.30 can be found.

$$COD(t) = COD_0 - \frac{I}{4\, F\, V}\, t \quad (2.30)$$

This behavior continues until a critical time (t_{cr}), which corresponds to the moment the applied current density reaches the limiting current density. At this time, Equation 2.31 may be used to calculate the COD critical value, where COD_{cr} is the critical COD, in mol O_2 m^{-3}.

$$COD_{cr} = \propto COD_0 = \frac{I}{4\, A\, F\, k_m} \quad (2.31)$$

Replacing Equation 2.31 in Equation 2.29, the critical time, in s, can be calculated by Equation 2.32:

$$t_{cr} = \frac{1 - \propto}{\propto}\, \frac{V}{A\, k_m} \quad (2.32)$$

- $j > j_{lim}$

The electrolysis is controlled by mass transport and, when secondary reactions like oxygen evolution are involved, the current efficiency is reduced. Due to mass transport limitation under these conditions, the removal of COD exhibits an exponential tendency. In these conditions, Equation 2.33 can be used to represent the temporal evolution of COD.

$$COD(t) = COD_0 \exp\left[-\left(\frac{A\,k_m}{V}\right) t\right] \quad (2.33)$$

The ICE can be defined by Equation 2.34, being the volume unit in L, COD_0 and COD units in g L^{-1} and 8 the oxygen equivalent mass.

$$ICE = \frac{j_{lim}}{j} = \frac{COD(t)}{\propto COD_0} = 100\,F\,V\left(\frac{COD(t) - COD_0}{8\,I\,t}\right) \quad (2.34)$$

Even though this model (Panizza et al., 2001) has demonstrated excellent agreement with experimental results in the electro-oxidation of synthetic solutions of single organic compounds by BDD anodes, it has also demonstrated deviations when dealing with complex mixtures where the existence of electrogenerated secondary oxidants also adds to the overall kinetics (Anglada et al., 2009).

It is well known that the EO process has no pH restrictions (Sirés et al., 2014) and is not easily affected by temperature (Moreira et al., 2017). In many cases, however, the solution's electrical conductivity (EC) must often be improved by the addition of a supporting electrolyte (Yavuz et al., 2012), which also helps to lower the energy cost. Chloride, sulfate, and persulfate salts are some of the electrolytes that are frequently utilized for this purpose; the influence of adding these electrolytes has already been investigated in WW remediation using EO processes (Candia-Onfray et al., 2018). Additionally, these salts can further help in the oxidation process through the formation of new oxidizing species at the anode. As aforementioned, Cl^- can react at the anode to create Cl_2, HClO and ClO^- (Eqs. 2.22–2.24), while sulfate and persulfate can generate the highly reactive sulfate radical ($SO_4^{\bullet -}$) through Equations 2.25, 2.35 and 2.36 (Fernandes et al., 2021).

$$2\,SO_4^{2-}\,(aq) \rightarrow S_2O_8^{2-}\,(aq) + 2\,e^- \quad (2.35)$$

$$S_2O_8^{2-}\,(aq) + e^- \rightarrow SO_4^{\bullet -}\,(aq) + SO_4^{2-}\,(aq) \quad (2.36)$$

Furthermore, additional sulfate radical electrogeneration may be carried out by sulfate ions direct oxidation (Eq. 2.37) and/or oxidation through a hydroxyl radical (Eq. 2.38), when using anode materials with high oxygen evolution potential, such as platinum, BDD, as well as some metal oxides like PbO_2 and SnO_2 (Fernandes et al., 2021).

$$SO_4^{2-}\ (aq) \rightarrow SO_4^{\bullet-}\ (aq) + e^- \quad (2.37)$$

$$SO_4^{2-}\ (aq) + HO^{\bullet}\ (aq) \rightarrow SO_4^{\bullet-}\ (aq) + HO^-\ (aq) \quad (2.38)$$

Supplementary hydroxyl radicals can be also obtained through sulfate radical reactions with water (Eq. 2.39), further enhancing the EO process (Fernandes et al., 2021).

$$SO_4^{\bullet-}\ (aq) + H_2O\ (l) \rightarrow SO_4^{2-}\ (aq) + HO^{\bullet}\ (aq) + H^+\ (aq) \quad (2.39)$$

The application of the EO process to winery wastewater treatment has been reported by some authors. Table 2.2 shows a compilation of these reports, with a summary of the main experimental conditions studied and the discoloration or COD/TOC removal obtained.

Stainless steel was the most used cathode material in these studies, while BDD was the preferred choice for the anode material, with most of the works that used this combination of electrodes obtaining a >90% mineralization rate.

As previously mentioned, Moreira et al. (2015) and Diez et al. (2016) studied the efficiency of electrochemical oxidation process for WW treatment in comparison with EF-like processes, and both found EO to be the least efficient electrochemical treatment process. This is due to the added benefits that the Fenton-based processes bring to the EO process.

Baía et al. (2022) studied the influence of applied current density in the EO treatment of WW with 5700 mg L^{-1} COD, applying current densities ranging from 300 to 900 A m^{-2}. Current densities higher than 500 A m^{-2} required the addition of a supporting electrolyte (0.25 g L^{-1} of Na_2SO_4), due to the low electrical conductivity of the WW. It was concluded that, even without the addition of a supporting electrolyte, the lowest applied current density (300 A m^{-2}) was able to match the degradation efficiency of the highest applied current density (900 A m^{-2}). Although the lowest current density studied took a longer time to reach the same mineralization rate, it still resulted in a lower specific energy consumption (47 kWh (kg COD)$^{-1}$ obtained at 300 A m^{-2} *vs* 88 kWh (kg COD)$^{-1}$ obtained at 900 A m^{-2}). This study also focused on the specific degradation of three recalcitrant compounds normally present in WW (phthalic acid, tyrosol, and catechin), with this process being able to achieve a 99.9% removal of these compounds.

Table 2.2 – A summary of the research results previously reported for the degradation of winery wastewater by electrochemical oxidation.

Anode / cathode	Inter-electrode gap / cm	COD_0 / mg L^{-1}	Applied current density / Potential	Operation time / h	Supporting electrolyte	COD/TOC removal or discoloration / %	References
BDD / carbon-PTFE	0.5	380	250 A m^{-2}	4	–	36 (TOC)	Moreira et al. (2015)
Graphite / graphite	8	14430	5 V	5.67	0.01 M (Na_2SO_4)	60 (discoloration)	Diez et al. (2016)
BDD / stainless steel	0.3	5700	300 A m^{-2}	14	–	98.3 (COD)	Baía et al. (2022)
			900 A m^{-2}	6	0.25 g L^{-1} (Na_2SO_4)	97.8 [a] (COD)	
BDD / stainless steel	1	4140	300 A m^{-2}	9	–	85 (TOC)	Lauzurique et al. (2022)
Ti/$Ir_{0.45}Ta_{0.55}O_2$ / stainless steel					–	3.34 (TOC)	
Ti/$Ru_{0.3}Ti_{0.7}O_2$ / stainless steel					–	1.70 (TOC)	
BDD / stainless steel	NS	3490	600 A m^{-2}	7	–	63.6 (COD)	Candia-Onfray et al. (2018)
					50 mM (NaCl)	92.1 [a] (COD)	
					50 mM (Na_2SO_4)	99.8 [a] (COD)	
BDD / stainless steel	NS	259	500 A m^{-2}	16	5 g L^{-1} (NaCl)	~71 [a] (COD)	Martínez-Cruz et al. (2020)
					5 g L^{-1} (Na_2SO_4)	~64 [a] (COD)	

[a] Value obtained indirectly from data presented in the article. NS – Not specified.

Lauzurique et al. (2022) studied the influence of the anode material in the treatment of a WW with 4140 mg L^{-1} COD. Two types of anodes were tested, a standard BDD electrode and two mixed metal oxide (MMO) electrodes. The obtained results showed that BDD was much more efficient than MMO in the degradation of WW, with 85% TOC removal, while MMO presented, in average, only 2.53% TOC removal. Being BDD a non-active anode, its weak interaction with $^{\bullet}OH$ and its high overpotential for oxygen evolution result in the production of more reactive physically absorbed BDD($^{\bullet}OH$) radicals, which mineralize the pollutants in the wastewater more efficiently (Lauzurique et al., 2022).

In a different study, Candia-Onfray et al. (2018) evaluated the influence of the supporting electrolyte, NaCl or Na_2SO_4, on the EO performance. The attempt to treat a WW with a COD of 3490 mg L^{-1} resulted in a 63.6 % COD removal when no electrolyte was used and 92.1 and 99.8% COD removal when NaCl and Na_2SO_4 were added, respectively. Large concentrations of sulfate and chloride promote the formation of oxidants such as hydroxyl and sulfate radicals (Eqs. 2.35–2.39) and active chlorine species (Eqs. 2.22–2.24), which react with organics in solution. When adding a supporting electrolyte to industrial wastewaters, it also boosts conductivity, lowers cell potential, and thus reduces the energy needed for EO process (Candia-Onfray et al., 2018).

Martínez-Cruz et al. (2020) also studied the influence of the supporting electrolyte (NaCl or Na_2SO_4) on the EO treatment of a WW with a COD of 259 mg L^{-1}. The authors observed a slightly higher COD removal with NaCl, when compared with the use of Na_2SO_4. This can be attributed to the low organic load of the WW, which would favor bulk oxidation, due to the lower amount of pollutant molecules reaching the anode surface. Indirect oxidation in the bulk of the solution can be better exploited by the oxidizing species produced from chloride (Eqs. 2.22–2.24) than by the ones produced from sulphate (Eqs. 2.35–2.39). Additionally, this study aimed to evaluate the efficiency of the EO process in other types of wastewaters, from which was concluded that when operating at high COD conditions, a higher process efficiency can be obtained (Martínez-Cruz et al., 2020).

Chapter 3 - Materials and methods

3.1 Winery wastewater

The winery wastewater used in this work was collected from a pond of a wine-producing family property. This pond receives the wastewater resulting from the grape-processing for wine production and from the washing of materials and equipment. The characterization of the WW is presented in Table 3.1. It was found that the organic load of the collected WW is very low compared to that described in the literature for winery effluents, which, according to Mosse et al. (2011), present an average COD of 15 g L^{-1}. Thus, to increase the organic load of the WW, the collected effluent was spiked with commercial wine, being the composition of the spiked effluent 97.5% WW and 2.5% commercial wine (V/V). The characterization of the spiked WW, used in the electrochemical experiments, is also presented in Table 3.1.

Table 3.1 – Characterization of the winery wastewater used in the electrochemical study, before and after being spiked with commercial wine.

Sample	Raw WW	Spiked WW
pH	6.93 ± 0.08	5.9 ± 0.7
Electrical conductivity / mS cm^{-1}	0.19 ± 0.02	1.1 ± 0.2
Chemical oxygen demand / g L^{-1}	0.226 ± 0.003	5.0 ± 0.2
Total carbon / g L^{-1}	0.073 ± 0.005	1.38 ± 0.07
Inorganic carbon / g L^{-1}	0.015 ± 0.009	0.03 ± 0.02
Total organic carbon / g L^{-1}	0.058 ± 0.007	1.35 ± 0.07
Total nitrogen / mg L^{-1}	< 5	< 5

3.2. Electrochemical degradation study

The WW spiked with commercial wine was treated by two different electrochemical processes, EF and EO. All the degradation experiments were conducted in batch mode, using an undivided cylindrical cell, containing 230 mL of spiked WW. During the experiments, the solution was continuously stirred, at 300 rpm, using a magnetic bar, to enhance the mass transport of reactants/products toward/from the electrodes. A GW, Lab DC, model GPS-3030D (0–30 V, 0–3 A) was used as the power supply.

3.2.1. Electro-Fenton experiments

For the EF experiments, the spiked WW was previously supplemented with iron and acidified at pH 3. As iron source, it was used iron(II) sulfate heptahydrate ($FeSO_4 \cdot 7H_2O$, Sigma-Aldrich, ≥ 99.0%). Two different iron concentrations were studied, 10 and 50 mg L^{-1}. To acidify the solution to pH 3, a concentrated solution of sulfuric acid was utilized.

A CF piece, purchased from Carbone Loraine, with a thickness of 0.5 cm and an immersed area of 110 cm^2, was used as cathode, and a BDD electrode, purchased from Neocoat, with an immersed area of 10 cm^2, was used as anode. The anode was placed in the center of the cell and surrounded by the cathode, which covered the inner wall of the cell. Figure 3.1 presents a schematic representation of the experimental setup utilized.

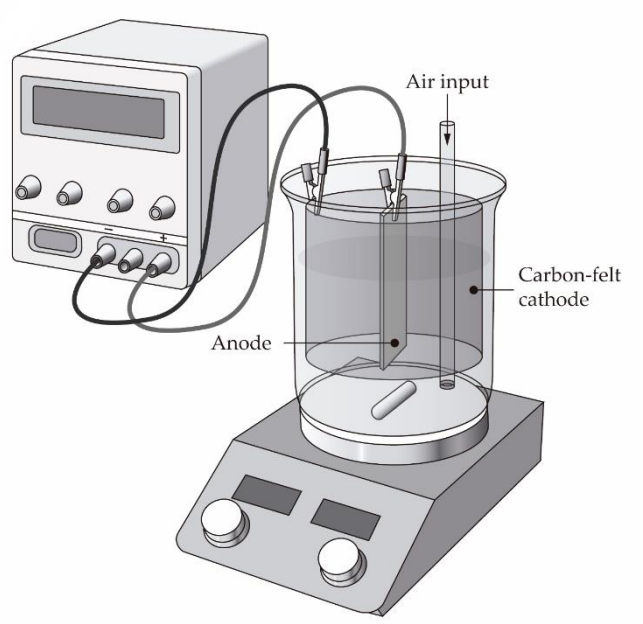

Figure 3.1 – Schematic representation of the experimental setup utilized in the electro-Fenton experiments.

Continuous O_2 saturation at atmospheric pressure was ensured by bubbling compressed air through a fritted glass diffuser at 1 L min^{-1}, starting 10 min before the experiment, to reach a steady O_2 concentration that allowed H_2O_2 electrogeneration. To verify that H_2O_2 was being properly produced and was enough to react with the iron, H_2O_2 determinations were performed.

The influence of the applied current intensity on the EF efficiency was assessed. A description of the different experimental variables combination is presented in Table 3.2.

Table 3.2 – Description of the different experimental variables' combination studied for EF process.

I / A	$[Fe^{2+}]$ / mg L^{-1}
0.1	10
0.3	10
	50

The duration of the experiments was 6 h, with samples being collected every 2 h for analytical determinations and experiments monitoring. The samples from the EF experiments were characterized through COD, total carbon (TC), inorganic carbon (IC), total organic carbon (TOC), total nitrogen (TN), total dissolved iron (TDI), dissolved Fe^{2+}, H_2O_2 concentration, pH, and electrical conductivity (EC) determinations.

3.2.2. Electro-oxidation experiments

The EO experiments were divided in two groups, according to the operational variables under study and the cell configuration utilized.

The first group of experiments focused on the influence of the type and concentration of electrolyte and of the applied current intensity in the degradation process. It was also evaluated if CF was a viable option as anode material for EO experiments, compared to the widely used BDD. As electrolyte, it was studied sodium sulfate anhydrous (Na_2SO_4, Sigma-Aldrich, ≥ 99.0%), sodium peroxodisulfate ($Na_2S_2O_8$, Sigma-Aldrich, ≥ 98%), and $Na_2S_2O_8$ combined with $FeSO_4 \cdot 7H_2O$. The experimental setup utilized was like that used at the EF experiments (Figure 3.1), but without the air input. The cathode consisted of a CF piece with an immersed area of 110 cm^2, as for the EF experiments. Regarding the anode material, BDD or CF, with an immersed area of 10 cm^2, were used. A detailed description of the different experimental variables combination is presented in Table 3.3. The duration of the experiments was 8 h, with samples being collected every 2 h for analytical determinations and experiments monitoring. The samples were characterized through COD, TC, IC, TOC, TN, pH, and EC determinations, and also by TDI, dissolved Fe^{2+}, and $S_2O_8^{2-}$ analysis, when applicable.

Table 3.3 – Description of the different experimental variables' combination studied in the first group of EO experiments.

Electrolyte	[Electrolyte] / g L^{-1}	I / A	Anode
–	–	0.1	BDD
			CF
Na_2SO_4	0.25	0.1	BDD
			CF
		0.5	BDD
	5	0.1	BDD
			CF
		0.5	BDD
			CF
$Na_2S_2O_8$	5	0.5	BDD
$Na_2S_2O_8$ +($FeSO_4 \cdot 7H_2O$ – 10 mg L^{-1} Fe^{2+})	5	0.5	BDD

The second group of EO experiments focused on the durability and reproducibility of CF as anode material, when compared to the reference material BDD. The influence of the applied current intensity was assessed. For these experiments, CF or BDD, with an immersed area of 10 cm^2, were used as anode material. As for the cathode material, a stainless steel plate or a CF piece, with a similar area to the anode, were utilized. Both anode and cathode were placed in the center of the electrochemical cell, parallel to each other, with a 1.5 cm gap between them (Figure 3.2).

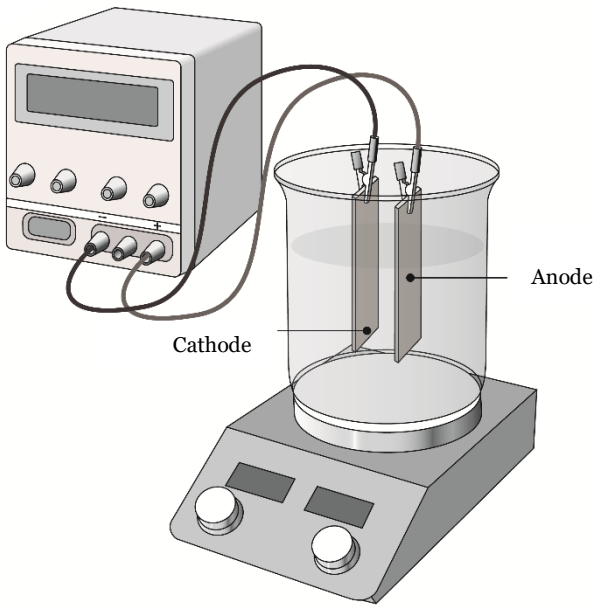

Figure 3.2 – Schematic representation of the experimental setup utilized in the electro-oxidation experiments.

The durability of the CF and reproducibility of the results was assessed through consecutive EO experiments utilizing the same pair of CF anode and cathode. Consecutive assays of 8 and 24 h duration were performed, being the effluent renewed between assays. Additionally, a sequence of 8 h duration assays was run, being the potential reversed between anode and cathode every 30 minutes. The sequences of assays were stopped when the CF anode could no longer stand. A detailed description of the different experimental variables combination studied in this group of EO experiments is presented in Table 3.4.

Table 3.4 – Description of the different experimental variables' combination studied in the second group of EO experiments.

Anode	Cathode	I / A	Assay duration
BDD	CF	0.1	8 h
CF	SS		8 h
CF	CF		8 h × 4 assays
			8 h (polarity reversal every 30 minutes) × 4 assays
			24 h × 2 assays + 12 h assay
		0.3	8 h

For the experiments with 8 h duration, samples were collected every 2 h for analytical determinations of COD, TC, IC, TOC, TN, pH, and EC. For the experiments run for 24 h, samples were only collected after the 24 hours.

For all the experiments run with CF anode, samples of the CF anode and of the CF cathode were collected after each assay, by cutting a small piece of the CF electrode from the most deeply immersed part, for characterization through scanning electron microscopy (SEM) and energy-dispersive X-ray spectroscopy (EDS).

3.3. Analytical methods

Several parameters were used to characterize the wastewater samples and to monitor the electrochemical experiments, namely COD, TC, TOC, IC, TN, pH, and EC. TDI, dissolved Fe^{2+}, H_2O_2 and $S_2O_8^{2-}$ determinations were also performed, through experimental techniques that make use of UV-visible absorption spectrophotometry.

The carbon felt electrodes utilized in the EO experiments were analyzed by SEM and EDS.

In the following subsections, it is presented a brief description of the analytical methods and equipment used to determine each parameter.

3.3.1 Chemical oxygen demand

The amount of organic matter in a sample can be indirectly measured by the analysis of COD, which, expressed in terms of oxygen concentration, represents the amount of oxygen that would be necessary to oxidize the organic matter content in the sample, by a strong oxidant. Thus, it is also an important parameter to evaluate the performance of the oxidation treatment in these samples. The basis for this parameter is that nearly all carbon content in organic compounds can be fully oxidized to carbon dioxide, by a strong oxidizing agent in acidic media.

The method used in this work for the determination of COD was the closed reflux titrimetric method, which involves the oxidation of the samples using excess dichromate, as described in Section 5220C of Standard Methods (Eaton et al., 2005). The digestion of the samples occurred in strongly acid solution with a known quantity of potassium dichromate ($K_2Cr_2O_7$, Panreac, 99%), that was in excess. Under these conditions, the organic matter is oxidized to CO_2 and H_2O, with the dichromate ion acting as the oxidizing agent, and being reduced to the chromic ion, according to Equation 3.1, in which c = (2/3)n + (1/6)a – (1/3)b:

$$C_nH_aO_b + 8c\ H^+ + c\ Cr_2O_7^{2-} \rightarrow 2c\ Cr^{3+} + \frac{a+8c}{2}\ H_2O + n\ CO_2 \quad (3.1)$$

The digestion also required a silver catalyst (Ag_2SO_4, Carlo Erba, 98.5%), to oxidize resistant organic compounds, and mercury sulfate ($HgSO_4$, Sigma Aldrich, 99%), to reduce interferences from chloride ion oxidation. The volume of sulfuric acid and silver sulfate solution was measured with a Socorex caliberx 520 meter. To homogenize the samples, a VWR VV3 vortex was used. Closed reflux digestion was performed using a Merck Spectroquant TR 420 thermoreactor, during 2 h at 150 ºC.

After digestion, the remaining unreduced dichromate was titrated with ferrous ammonium sulfate (FAS) solution ($(NH_4)_2Fe(SO_4)_2.6H_2O$, Panreac, 99-100%), using ferroin ($C_{12}H_8N_2.H_2O$, Sigma Aldrich, ≥ 99.5%) as color indicator, to determine the amount of dichromate consumed. The titration was performed using a Metrohm 876 Dosimat Plus automatic titrator. The reaction between dichromate and FAS follows Equation 3.2:

$$Cr_2O_7^{2-} + 14\ H^+ + 6\ Fe^{2+} \rightarrow 2\ Cr^{3+} + 7\ H_2O + 6\ Fe^{3+} \quad (3.2)$$

The dichromate consumed by the sample, which is calculated from the amount of unreduced dichromate, is equivalent to the amount of oxygen needed to oxidize the organic matter. The COD, expressed in milligrams of oxygen per liter of sample, was then determined.

3.3.2 Total, organic, and inorganic carbon

Total carbon corresponds to the dissolved amount of carbon (organic and inorganic) in a sample, expressed in concentration of carbon. Unlike COD, TC is independent of the oxidation state of organic matter. It is a global parameter that allows the evaluation of the degradation efficiency of wastewater treatment.

In the present work, TC was determined by the high temperature combustion method, described in Section 5310B of Standard Methods (Eaton et al., 2005).

The TC, TOC, and IC determinations were performed in a Shimadzu TOC-VCPH carbon analyzer. In this equipment, the sample is injected, through an automated process, into a quartz combustion chamber at 680ºC, containing a platinum catalyst in an oxygen-rich atmosphere. The water is vaporized, and the carbon of the sample is oxidized to CO_2 and H_2O. The gas phase, containing the CO_2, is transported in the carrier gas through a moisture trap and halide scrubbers, to remove water vapor and halides from the gas stream before it reaches a non-dispersive infrared detector (NDIR), which measures the concentration of CO_2. IC is determined by injecting the sample into a reaction chamber where it is acidified, and all the inorganic carbon is converted into CO_2 (and H_2O), which is carried to the NDIR and measured.

The obtained TC and IC values are the average of, at least, two measurements, and are given directly by the equipment in mg C L^{-1}, together with TOC, which is determined by subtracting IC from TC. Regularly, calibration curves were performed with standard potassium hydrogen phthalate solutions ($C_8H_5KO_4$, Sigma Aldrich, ≥ 99.5%) for TC determinations, and a solution of sodium bicarbonate ($NaHCO_3$, Sigma Aldrich, ≥ 99.5%) and sodium carbonate (Na_2CO_3, Sigma Aldrich, ≥ 99.5%) for IC determinations.

3.3.3 Total nitrogen

Total nitrogen corresponds to the total amount of nitrogen (organic and inorganic) in a sample, expressed in concentration of nitrogen.

In the present work, TN was determined using a Shimadzu TNM-1 unit coupled to a Shimadzu TOC-VCPH analyzer. In this equipment, all the nitrogen present in the samples is first converted to nitrogen monoxide and nitrogen dioxide, by catalytic combustion in the furnace. Then the nitrogen species react with ozone, to form an excited state of nitrogen dioxide. Upon returning to ground state, the emitted light energy is measured, using a chemiluminescence detector, and converted to TN.

The obtained TN values are the average of, at least, two measurements, and are given directly by the equipment in mg N L^{-1}. Regularly, calibration curves are performed with standard potassium nitrate solutions (KNO_3, Sigma Aldrich, ≥ 99.5%).

3.3.4 pH

The pH of the samples, at 25 ºC, was measured using a pH meter Mettler Toledo SevenEasy.

3.3.5 Electrical conductivity

Electrical conductivity, or simply conductivity, is a measure of the ability of an aqueous solution to conduct an electric current. This ability depends on the presence of ions, and their total concentration and mobility. It is also influenced by the temperature. In this work, the conductivity of the samples was measured, at 25 ºC, using a conductivity meter Mettler Toledo SevenEasy S30K.

3.3.6 Total dissolved iron and dissolved iron(II)

The concentrations of TDI and dissolved Fe^{2+} were determined through a spectrophotometric method with 1,10-phenanthroline, according to ISO 6332:1988. This method is based on the reaction of Fe^{2+} with 1,10-phenanthroline in an acidic medium, which results in the formation of a red-orange complex, with maximum absorbance at 511 nm, that obeys the Lambert-Beer law.

For the determination of the dissolved Fe^{2+}, 0.5 mL of 1 g L^{-1} 1,10-phenanthroline ($C_{12}H_8N_2.H_2O$, Sigma Aldrich, ≥ 99.5%) solution and 0.5 ml of acetate buffer solution pH 3.3 were added to 2 ml of the sample to be analyzed. After 15 min of reaction, the absorbance was measured at 511 nm. For the determination of TDI, a small portion of ascorbic acid ($C_6H_8O_6$, Sigma-Aldrich, 99%) was added to the previous mixture, to reduce Fe^{3+} to Fe^{2+}, according to Equation 3.3 (Elmagirbi et al., 2012):

$$2\ Fe^{3+} + C_6H_8O_6 \rightarrow 2\ Fe^{2+} + C_6H_6O_6 + 2\ H^+ \quad (3.3)$$

After 15 min of reaction, the absorbance was measured at 511 nm.

The absorbance of the samples was measured with and without the addition of the method reagents and the difference between the values was converted into the concentrations of Fe^{2+} and TDI, to remove possible interferences from the sample matrix.

Calibration curves were performed with standard FAS solutions ($(NH_4)_2Fe(SO_4)_2.6H_2O$, Panreac, 99-100%) to obtain the linear relationships between the concentrations of Fe^{2+}/TDI and the absorbance at 511 nm (Figure 3.3). These linear relationships are translated by Equations 3.4 and 3.5 respectively:

$$[Fe^{2+}] = \frac{Abs + 0.0082}{0.1012} \quad (3.4)$$

$$[TDI] = \frac{Abs - 0.0106}{0.1033} \quad (3.5)$$

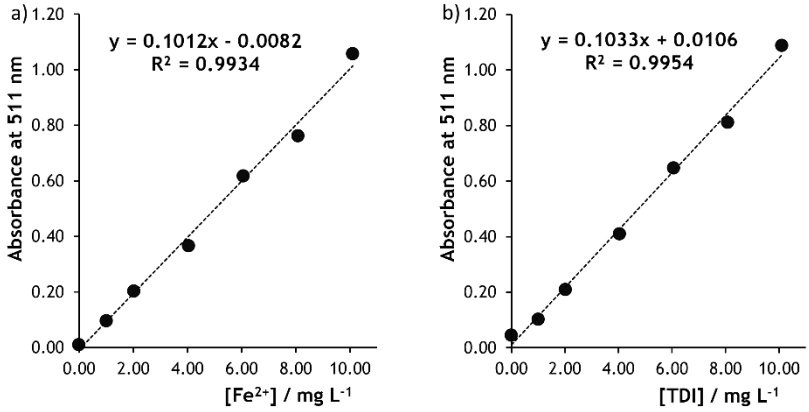

Figure 3.3 – Linear relationship between absorbance at 511 nm and the concentration of a) Fe^{2+} and b) TDI.

3.3.7 Hydrogen peroxide

The concentration of H_2O_2 was determined through a spectrophotometric method with metavanadate, as described by (Nogueira et al., 2005). This method is based on the reaction of H_2O_2 with ammonium metavanadate (NH_4VO_3, Merck, ≥ 99.0%), in an acidic medium, resulting in the formation of an orange-red peroxovanadium complex, with maximum absorbance at 450 nm, that obeys the Lambert-Beer law.

For the determination of H_2O_2, 1 mL of sample and 1 mL of 0.06 mol L^{-1} ammonium metavanadate solution in acidic medium were added in a 10 mL volumetric flask, which was then filled with deionized water. After 15 min of reaction, the absorbance of this solution was measured at 450 nm.

The absorbance of the experimental samples was measured with and without the addition of the metavanadate and the difference between the values was converted into the concentrations of H_2O_2, to remove possible interferences from the sample matrix.

Calibration curves were performed with commercial H_2O_2 solutions to obtain the linear relationships between the concentration of H_2O_2 and the absorbance at 450 nm (Figure 3.4). This linear relationship is translated by Equation 3.6:

$$[H_2O_2] = \frac{\text{Abs} - 0.021}{0.001} \quad (3.6)$$

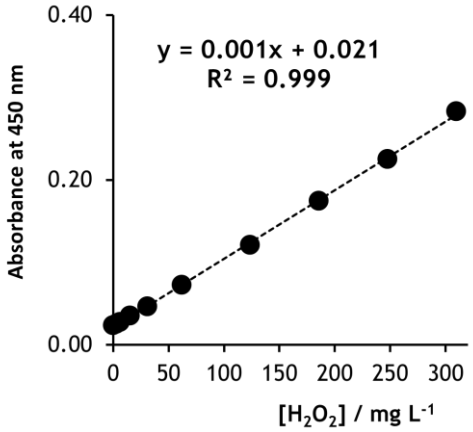

Figure 3.4 – Linear relationship between absorbance at 450 nm and the concentration of H_2O_2.

3.3.9 Scanning electron microscopy

SEM allows the morphological characterization of materials. The analysis of samples through this technique is generally performed under high vacuum conditions ($P \approx 10^{-4}$ Pa) and requires the sample to maintain physical and chemical stability under observation conditions (interaction of the electron beam with the sample). Using the scanning electron microscope, the surface of the sample is scanned by a finely focused electron beam, which reaches a very small area at a time. An image is obtained on the monitor, corresponding to the signal emitted by the detector for each analyzed point.

The emission of secondary electrons or electrons of low energy (< 50 eV) provides superficial results for a few tens of nanometers in depth, referring to the thickness of the sample to be analyzed, originating an image with a strong topographic contrast, with a clear view of the sample.

The analysis by backscattered electrons, with energy higher than the secondary electrons, corresponds to a result related to a deeper layer of the sample (hundreds of nanometers). The resolution of the images essentially depends on the energy of the incident beam and the local average atomic number of the material.

The measurements were performed using an EDX Bruker equipment with a voltage of 20 kV, coupled to a Hitachi S3400N Scanning Electron Microscope.

Chapter 4 – Results and Discussion

With the aim of evaluating the potential of carbon felt as electrode material in the electrochemical treatment of winery wastewater, several assays were performed, with two different electrochemical processes being used, electro-Fenton and electrochemical oxidation. In this chapter, the results of said assays are presented and discussed, with a chapter subdivision concerning the electrochemical process under study.

4.1. Electro-Fenton experiments

In the EF experiments, a BDD anode and CF cathode were utilized to evaluate the influence of the applied current intensity and of the initial concentration of Fe^{2+} on the process, with results being presented in Figures 4.1–4.3.

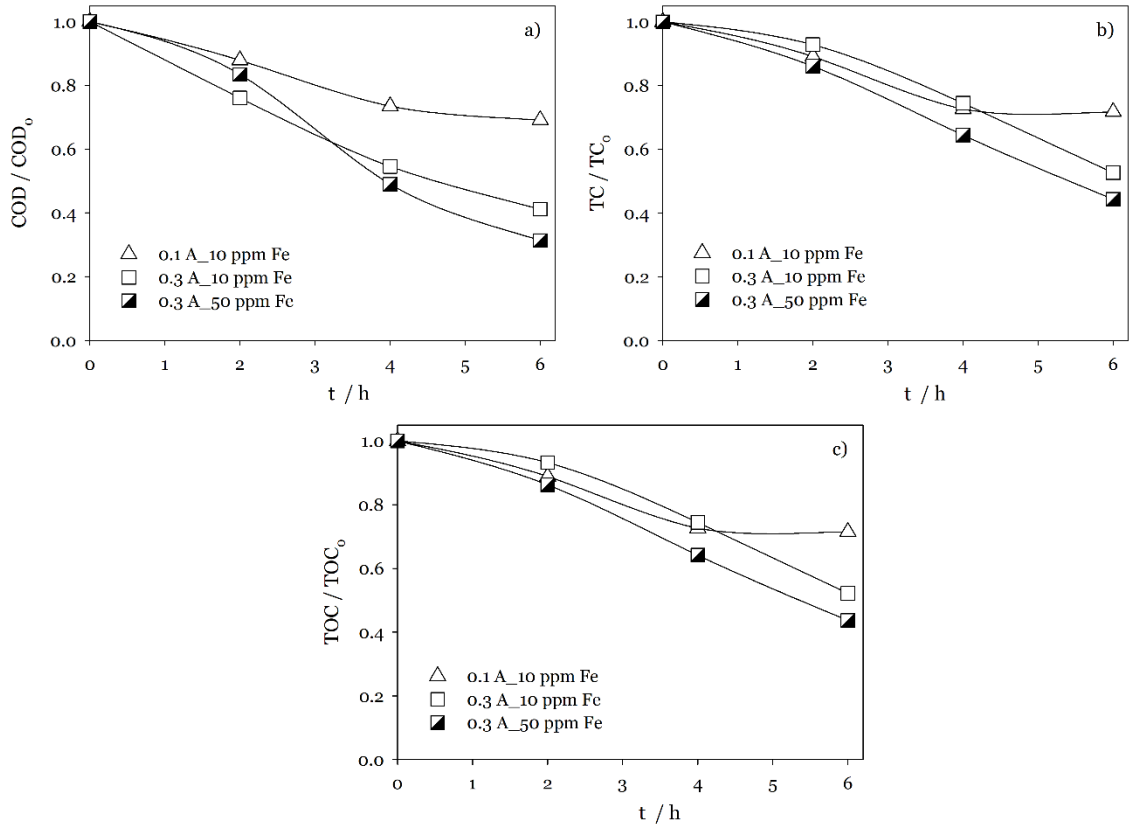

Figure 4.1 – Relative variation of (a) COD, (b) TC, and (c) TOC with time for the EF assays performed with winery wastewater.

It can be seen in Figure 4.1 that the EF process was successful in partially treating the winery wastewater, with the biggest organic load removal (69% COD) happening on the assay with the highest applied current intensity and Fe^{2+} concentration.

Concerning the influence of the applied current intensity, COD removal increased with applied current intensity (31% *vs* 59% at 0.1 A and 0.3 A, respectively), which should be the result of a larger generation of hydroxyl radicals. Meanwhile, the influence of the increase in initial Fe^{2+} concentration wasn't so noticeable, but it still proved beneficial to the process (59% *vs* 69% COD removal at 10 ppm Fe and 50 ppm, respectively), which can also be attributed to an increase in hydroxyl radicals generation, through Equation 2.1. TOC and TC present similar results since IC was irrelevant, i.e., IC was approximately 10% of TC.

In Figure 4.2.a), it can be seen that the amount of Fe^{2+} introduced in the process was almost depleted in the 6 hours of the assays, which should be due to the precipitation of iron salts (Equation 4.1) or cathodic electrodeposition of iron ions, since total iron concentration (Figure 4.2.b) also decreased (Coetzee et al., 2017).

$$Fe(OH_2)_6^{3+}\ (aq) \rightarrow Fe(OH)_n(OH_2)_{6-n}^{3-n}\ (aq) + n\ H^+\ (aq) \quad (4.1)$$

H_2O_2 concentration remained mostly around the same values throughout the experiment (Figure 4.2.c), possibly due to an equilibrium reached between the H_2O_2-depleting reactions (Equations 2.1, 2.14 and 4.2) and the H_2O_2-producing reactions (Equations 2.10, 4.3 and 4.4).

$$HO^{\bullet}\ (aq) + H_2O_2\ (l) \rightarrow HO_2^{\bullet}\ (aq) + H_2O\ (l) \quad (4.2)$$

$$Fe^{2+}\ (aq) + HO_2^{\bullet}\ (aq) + H^+\ (aq) \rightarrow Fe^{3+}\ (aq) + H_2O_2\ (l) \quad (4.3)$$

$$2\ HO_2^{\bullet}\ (aq) \rightarrow H_2O_2\ (l) + O_2\ (g) \quad (4.4)$$

The conductivity rised throughout the experiment (Figure 4.3.a), due to the formation of ionic species from the oxidation of the organic matter, which in turn led to an electrical potential drop (Figure 4.3.b).

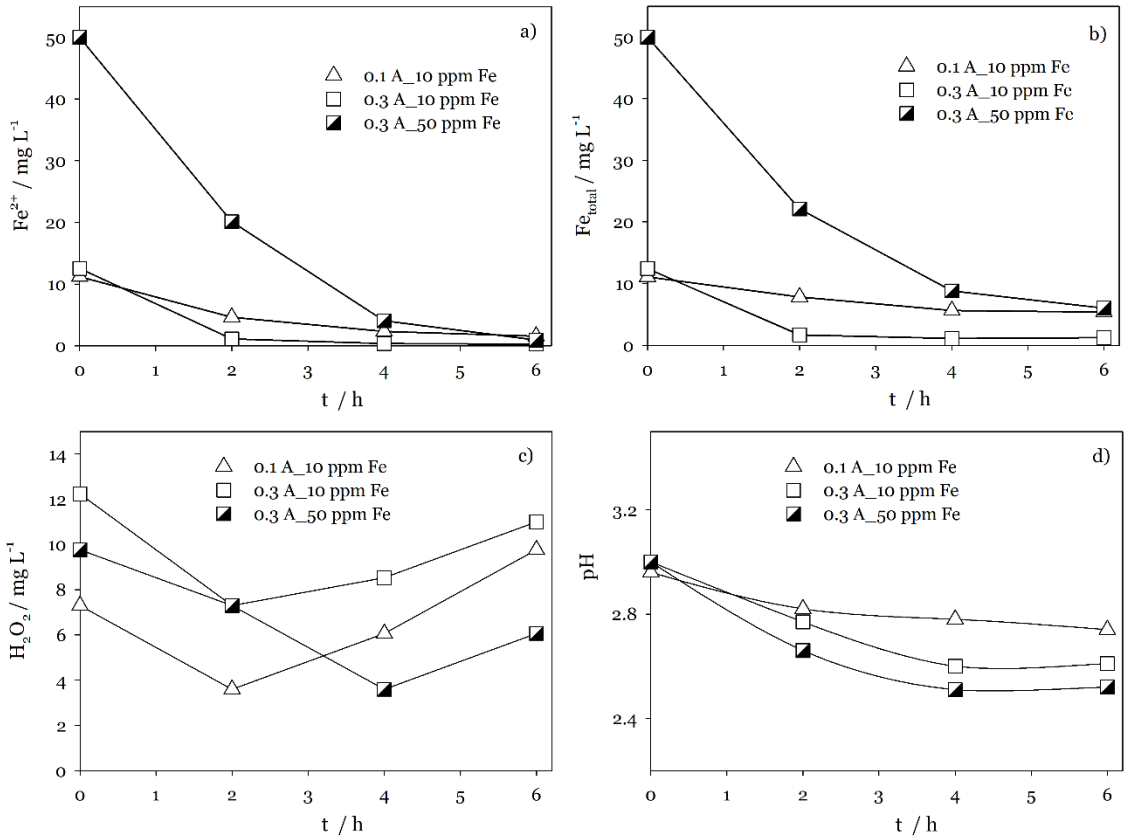

Figure 4.2 – Variation of (a) Fe^{2+} concentration, (b) Fe_{total} concentration, (c) H_2O_2 concentration, and (d) pH with time for the EF assays performed on winery wastewater.

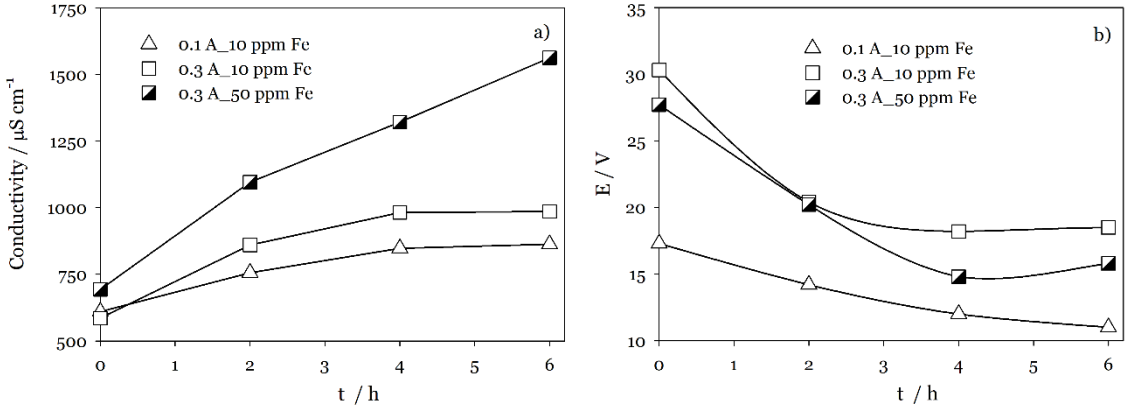

Figure 4.3 – Variation of (a) conductivity, and (b) potential with time for the EF assays performed on winery wastewater.

4.2. Electro-oxidation experiments

In the first group of EO experiments, the influence of the type and concentration of electrolyte and of the applied current intensity were evaluated, with results being presented in Figures 4.4–4.6.

It can be seen in Figure 4.4 that the EO process with a BDD anode was successful in treating the winery wastewater, with the highest COD removal (95%) observed for the assay performed at 0.5 A with added $Na_2S_2O_8$ and $FeSO_4{\cdot}7H_2O$.

The type of supporting electrolyte and its concentration didn't significantly influence the COD removal: 92% *vs* 92% with added Na_2SO_4 and $Na_2S_2O_8$, respectively, at 0.5 A; 31% *vs* 33% with 0 mg L^{-1} and 5 mg L^{-1} of added Na_2SO_4, respectively, at 0.1 A. The added $FeSO_4{\cdot}7H_2O$ didn't show a significant increase in the COD removal either: 95% *vs* 92% with and without added $FeSO_4{\cdot}7H_2O$, respectively). Contrariwise, the applied current intensity greatly affected the EO performance, with increases of around 60% COD removal being observed between the assays at 0.1 A and 0.5 A. This can be explained by the increase in the production of adsorbed hydroxyl radicals through Equation 2.15.

In Figures 4.4.e and 4.4.f, it can be seen that there was an initial decrease of IC in almost all the assays, followed by a plateau throughout the rest of the experiments, which should be due to an equilibrium reached between the oxidation of inorganic carbon and the conversion of the CO_2 subsequently produced into bicarbonate (HCO_3^-) and carbonate (CO_3^{2-}), through Equations 4.5–4.7.

$$CO_2\ (g) \leftrightarrow CO_2\ (aq)^* \quad (4.5)$$

$$CO_2\ (aq)^* + H_2O\ (l) \leftrightarrow H^+\ (aq) + HCO_3^-\ (aq) \quad (4.6)$$

$$HCO_3^-\ (aq) \leftrightarrow H^+\ (aq) + CO_3^{2-}\ (aq) \quad (4.7)$$

*dissolved gaseous CO_2

Following these reactions, a pH drop is expected to succeed the drop in IC, due to H^+ formation (Equations 4.6 and 4.7), which can be verified in Figures 4.5.a) and 4.5.b).

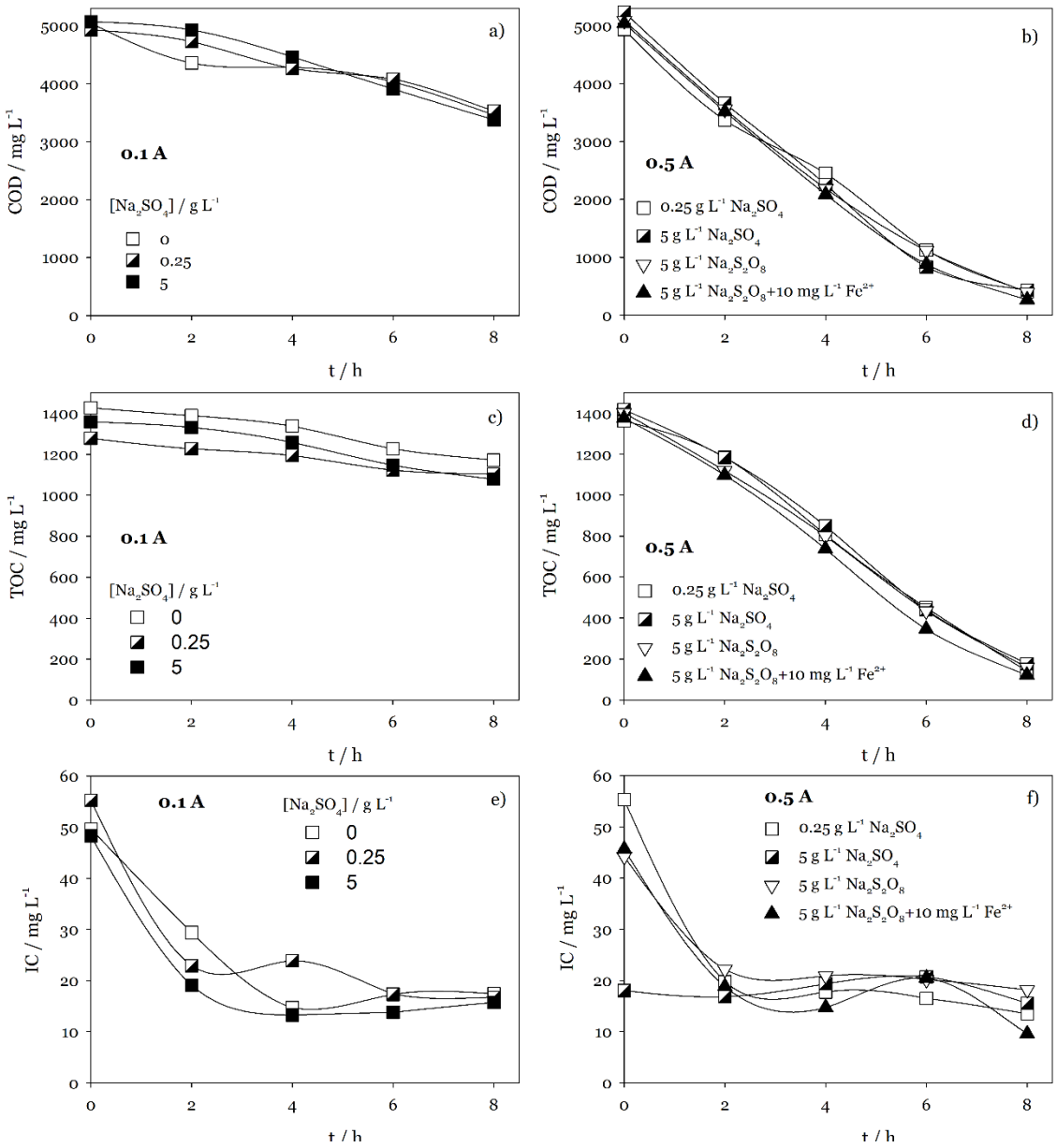

Figure 4.4 – Experimental results of EO assays with a BDD anode: Variation of (a) COD, (c) TOC, and (e) IC with time for experiments at 0.1 A; Variation of (b) COD, (d) TOC, and (f) IC with time for experiments at 0.5 A.

A significant decrease in pH and increase in electrical conductivity was observed during the first two hours of the experiments performed with added persulfate (Figures 4.5.b and 4.5.d). According to the literature, this decrease in pH and increase in electrical conductivity can be explained by the occurrence of the reactions in Equations 2.36, 2.39, and 4.8, which promote the production of H^+ and the persulfate dissociation into sulfate ion and sulfate radical (Malakootian & Ahmadian, 2019).

$$2S_2O_8^{2-}\,(aq) + 2H_2O\,(l) \leftrightarrow 4H^+\,(aq) + 4SO_4^{2-}\,(aq) + O_2\,(g) \quad (4.8)$$

For the assay with 5 g L^{-1} of added Na_2SO_4 at 0.5 A, the initial IC value is much lower than the initial values observed for the other assays (Figures 4.4.f). Accordingly, the initial pH of this assay is lower than that for the other assays. A possible explanation for this fact is a contamination of the sample by the sample tube.

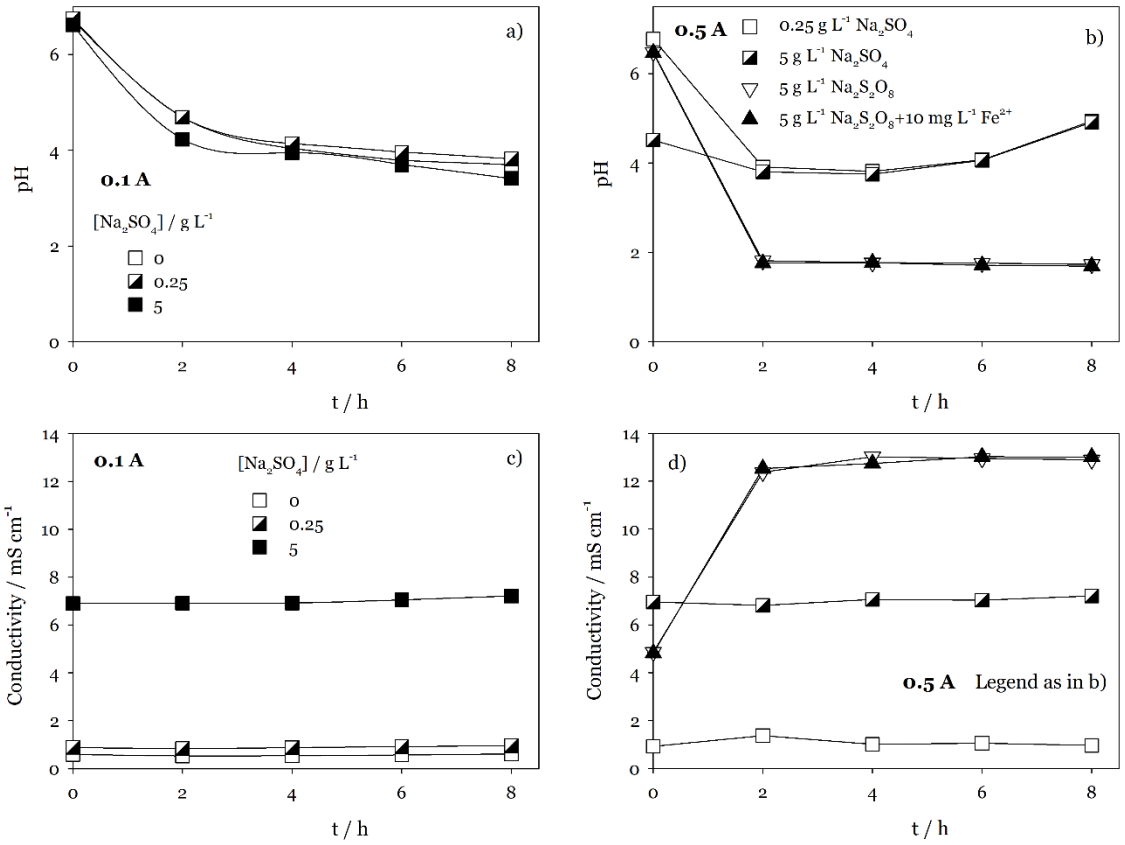

Figure 4.5 – Experimental results of EO assays with a BDD anode: Variation of a) pH; c) conductivity with time for experiments with 0.1 A; Variation of b) pH; d) conductivity with time for experiments with 0.5 A.

Figure 4.6 presents the experimental results obtained from the assays performed with carbon felt as anode material. It can be observed that EO with a carbon felt anode can partially treat the winery wastewater, with the highest COD removal (57%) happening on the assay at 0.5 A and added Na_2SO_4. This experiment did however stop prematurely, at the 6-hour mark, with the potential difference reaching the power source limit for current control.

As observed for the EO assays with BDD anode, the amount of electrolyte didn't seem to significantly influence the COD removal (27% *vs* 27% COD removal at 0 mg L^{-1} and 5 mg L^{-1} of added Na_2SO_4 at 0.1 A, respectively). Applied current intensity did, however, increase the COD removal (27% *vs* 57% COD removal at 0.1 A and 0.5 A, respectively), which, as described above, can be attributed to an increase in the production of adsorbed hydroxyl radicals, through Equation 2.15.

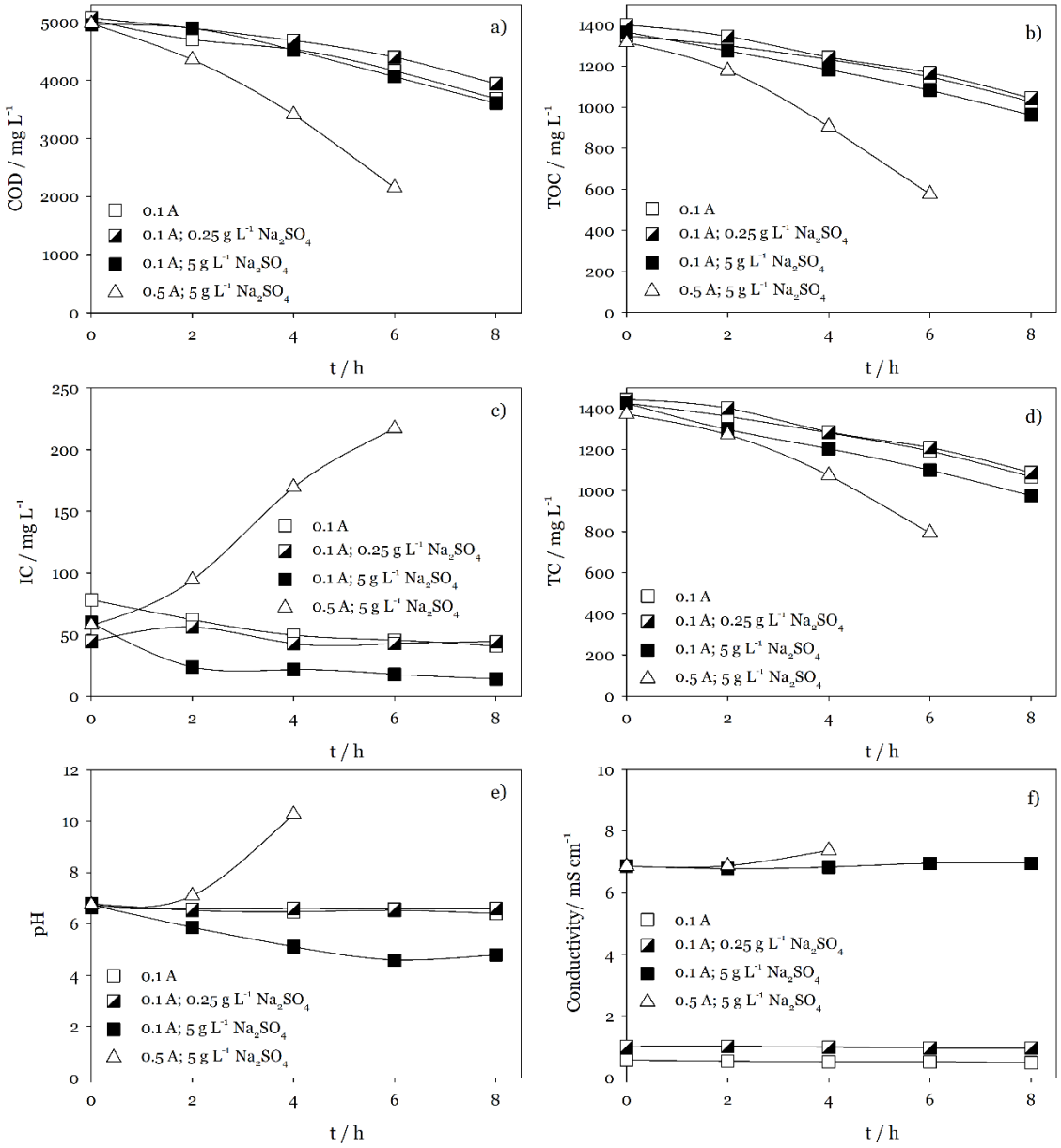

Figure 4.6 – Variation with time of different parameters during EO assays with a carbon felt anode: a) COD; b) TOC; c) IC; d) TC; e) pH; f) conductivity.

The second part of the experiments started by studying the performance of different electrode combinations in the treatment of WW, with results being presented in Figures 4.7 and 4.8.

It can be observed that, at 0.1 A, the pair BDD/CF presented better results than the pair CF/CF (32% *vs* 23% COD removal with BDD and CF anodes, respectively), while stainless steel is a slightly better cathode than CF (23% *vs* 28% COD removal with CF/CF and CF/SS, respectively). Carbon felt has the advantage of being much cheaper than BDD, which can compensate for its smaller removal capacity.

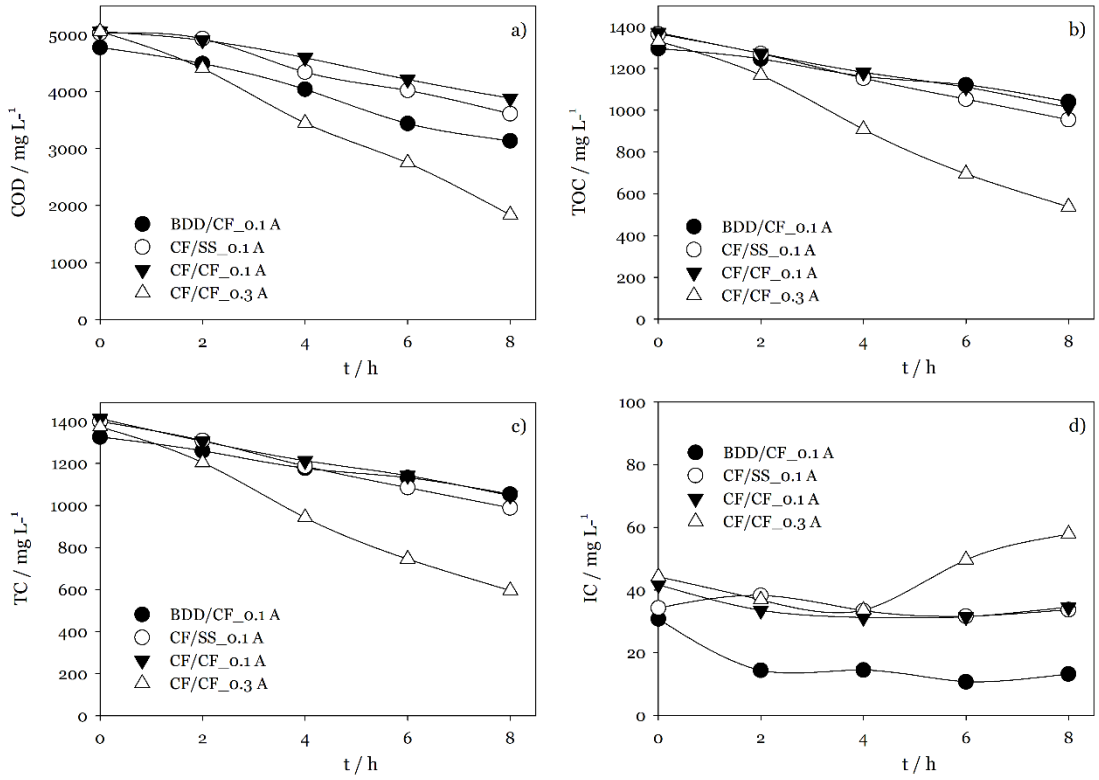

Figure 4.7 – Experimental results for the EO assays performed with different electrode combinations and applied current intensity: a) COD; b) TOC; c) TC; d) IC.

A higher current intensity resulted in a higher COD removal for CF/CF pair (23% *vs* 64% COD removal at 0.1 A and 0.3 A, respectively). Assuming the process was under current control, it is reasonable that a higher applied current intensity would promote a larger electron flux and consequently produce more hydroxyl radicals (Equation 2.1) to aid in the organic removal efficiency.

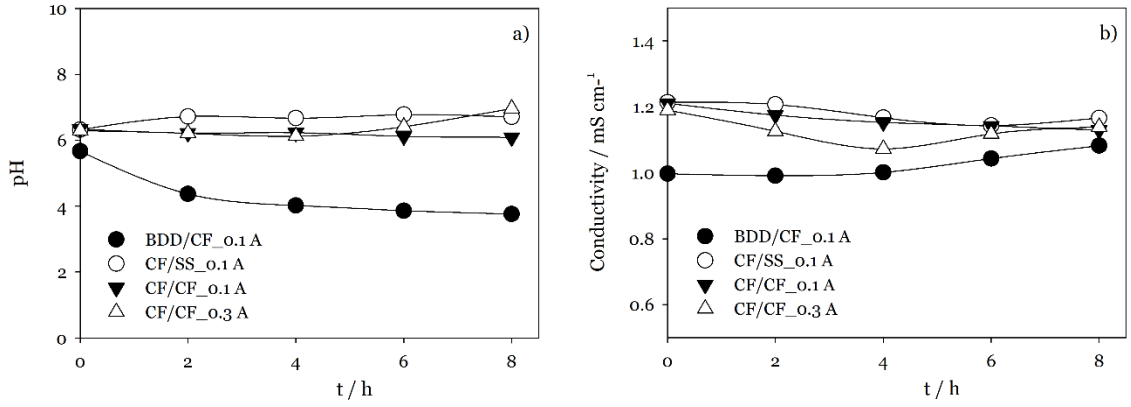

Figure 4.8 – Experimental results for EO assays run with different electrode combinations and applied current intensity: a) pH; b) conductivity.

A pH decrease can be observed on the assay using BDD as anode, probably due to a larger electrogeneration of hydroxyl radicals, typical of BDD anodes, which in turn produces a larger amount of H^+ through Equation 2.19.

To evaluate the degradation of the CF anode, a portion of the anode, before and after the assay with stainless steel, was analyzed through SEM (Figure 4.9).

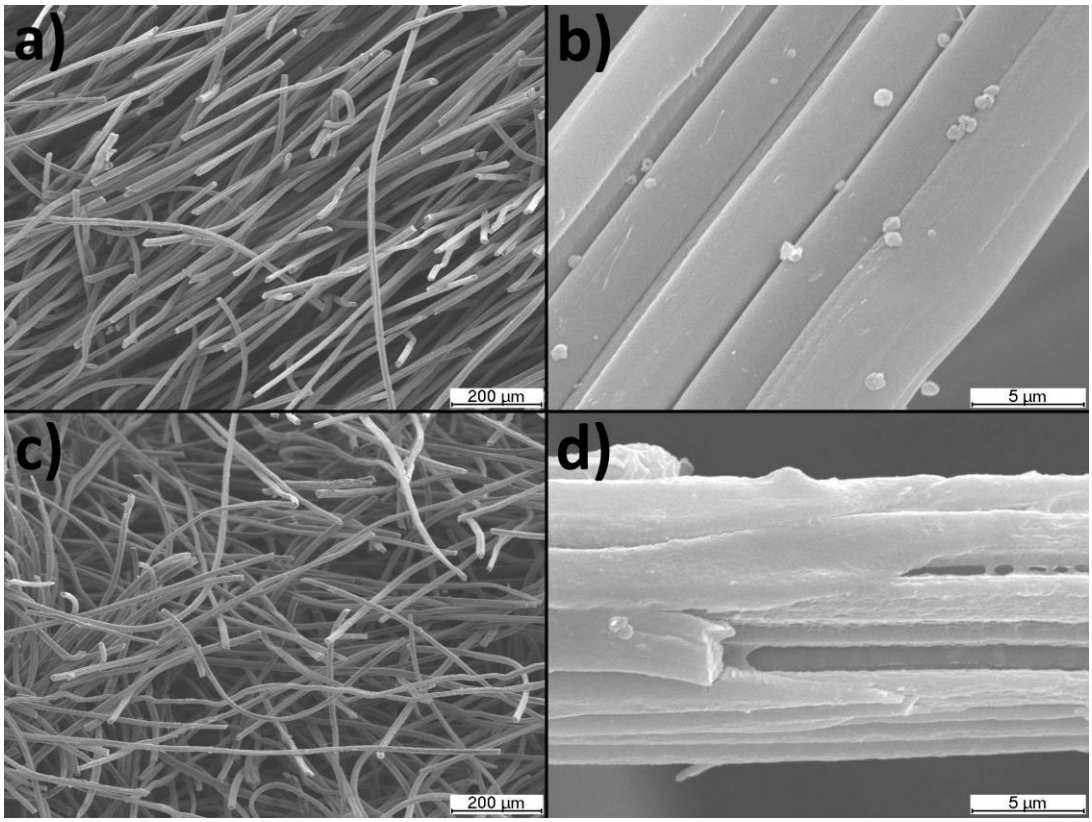

Figure 4.9 – SEM results of the analysis of the CF anode in the assay with a SS cathode: a) before the assay - 100x amplification; b) before the assay - 5000x amplification; c) after the assay - 100x amplification; d) after the assay - 5000x amplification.

It can be observed that, throughout the experiment, the anode suffered some type of degradation, with noticeable rupture of some of its fibers and a general loss of fiber density.

The durability and reproducibility of the results obtained with CF anode was evaluated through two series of experiments, one with the normal current flow and a second where the current flow was reversed every 30 minutes. Both series of experiments used the same pair of electrodes throughout four assays of 8-hour duration each, being the wastewater renewed between assays, to evaluate the durability and reproducibility of the CF anode. The experimental results obtained are presented in Figures 4.10–4.15.

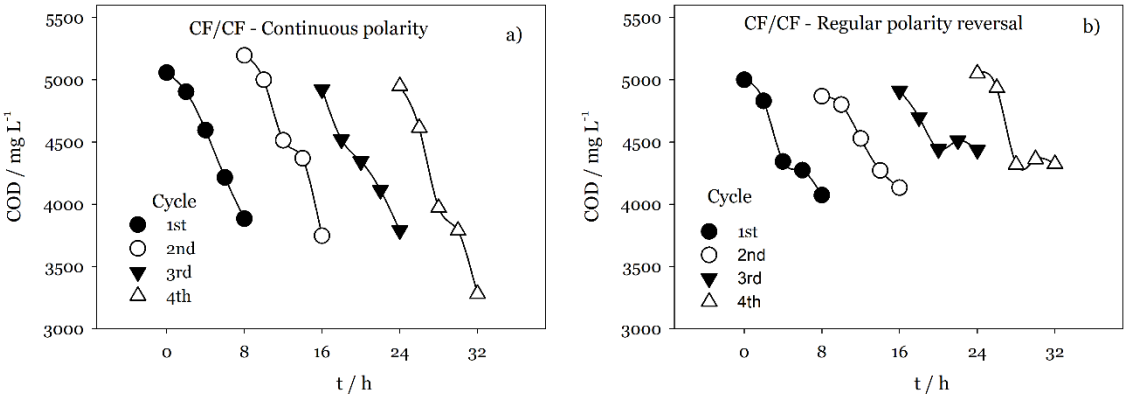

Figure 4.10 – Variation of COD with time for the experiments run at (a) continuous polarity, and (b) polarity reversal.

CF anode presented good reproducibility regarding COD removal, especially at continuous polarity, where no decrease in the performance was found throughout the four assays (1st: 23%; 2nd: 28; 3rd: 23%; 4th: 34%). Due to the breakage of the CF anode during the washing step after the 4th experiment, it was not possible to further continue this study. This puts in question the durability of the CF anode, which required further study.

TC and TOC (Figures 4.11 and 4.12, respectively) presented similar trend, probably because IC concentration is very low and with no expression on the results. TOC and COD decays are alike, showing constant combustion efficiency throughout experiments. IC (Figure 4.13) and pH (Figure 4.14) variations are related, as the increase in pH is probably due to the formation of bicarbonate and carbonate ions (Equations 4.6 and 4.7). This is much more relevant in the third and fourth cycles of the assays run at continuous polarity. A slight drop in conductivity (Figure 4.15) can be observed throughout the experiments, which could be prevented with regular addition of a supporting electrolyte.

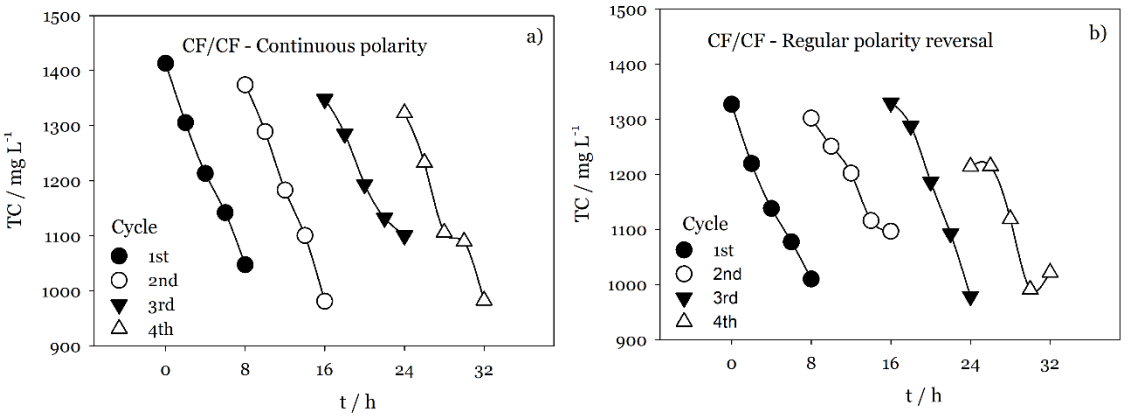

Figure 4.11 – Variation of TC with time for the assays performed at (a) continuous polarity, and (b) polarity reversal.

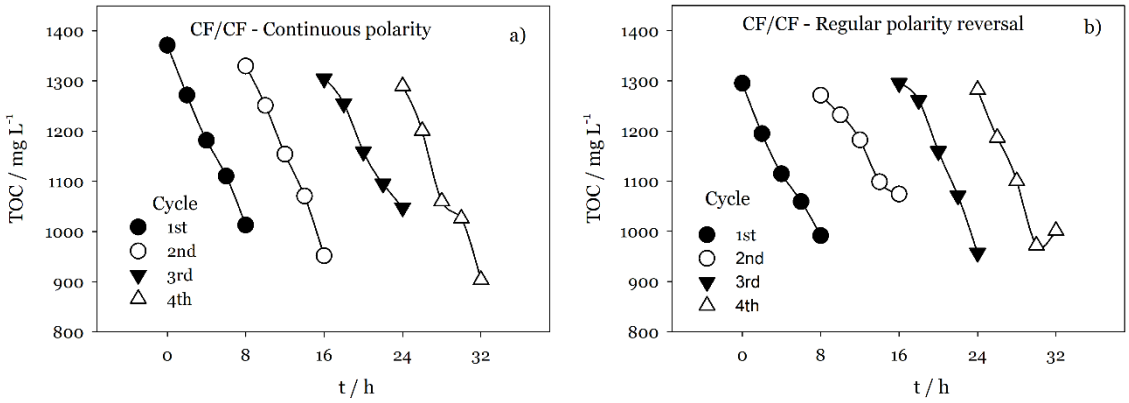

Figure 4.12 – Variation of TOC with time for the assays performed at (a) continuous polarity, and (b) polarity reversal.

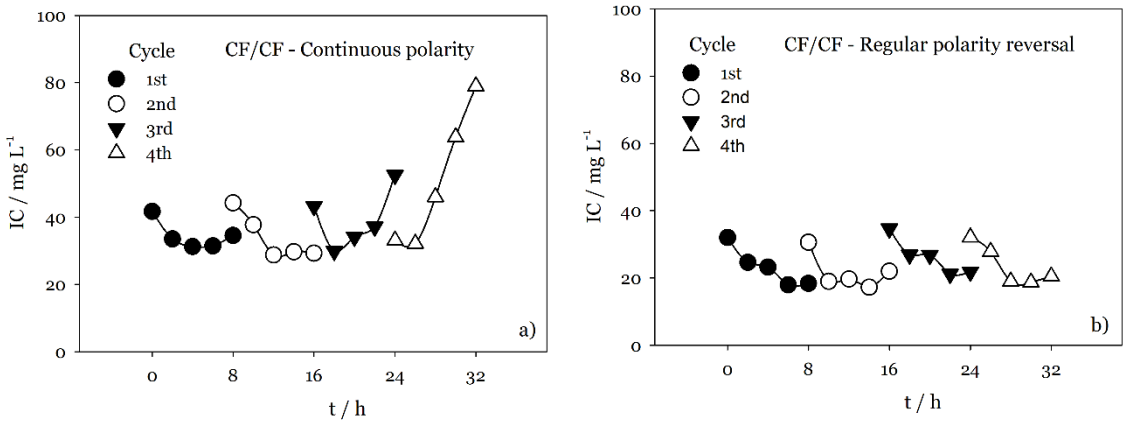

Figure 4.13 – Variation of IC with time for the assays performed at (a) continuous polarity, and (b) polarity reversal.

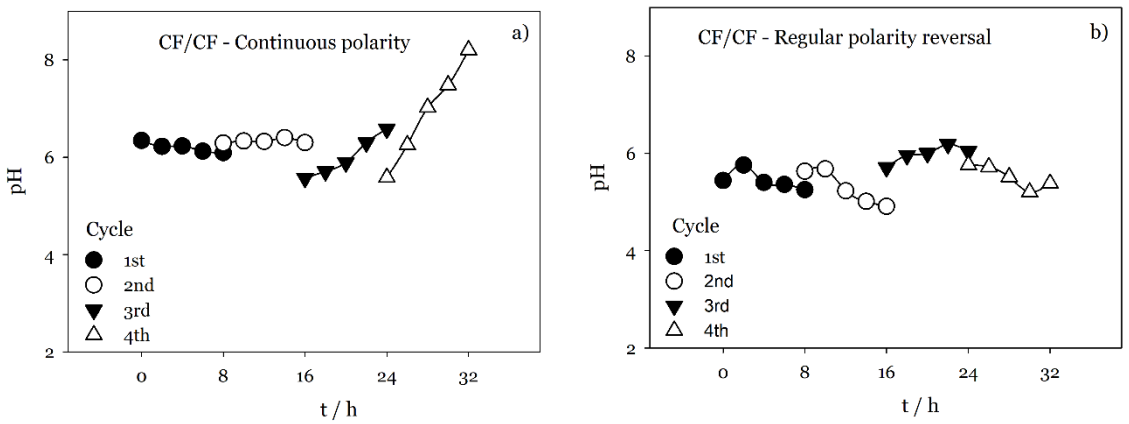

Figure 4.14 – Variation of pH with time for the assays performed at (a) continuous polarity, and (b) polarity reversal.

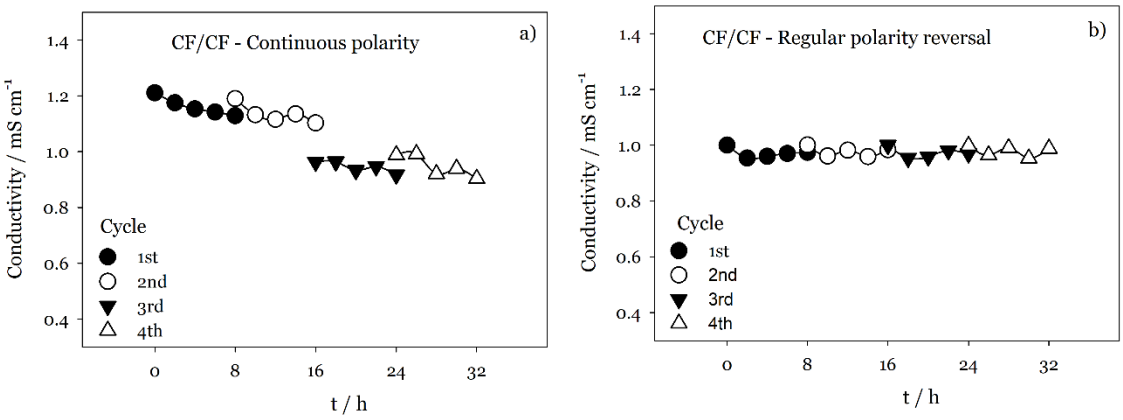

Figure 4.15 – Variation of conductivity with time for the assays performed at (a) continuous polarity, and (b) polarity reversal.

The degradation of the CF electrodes utilized in these experiments was assessed via SEM analysis (Figures 4.16–4.19). In the assays run at continuous polarity, it can be observed that both the anode and the cathode suffered erosion throughout the multiple cycles of the experiment, with noticeable aggravation of the damage on later cycles, which eventually led to the breakage of the CF piece at the end of the fourth cycle.

Although some fiber breakage can be observed in the assays run with polarity reversal, it is also noticeable that some form of deposition has occurred throughout the experiments. If this deposition clogged up the active sites of the CF fibers, then it could explain the lower removal efficiency shown with polarity reversal (27% *vs* 14% average COD removal with continuous polarity and polarity reversal, respectively).

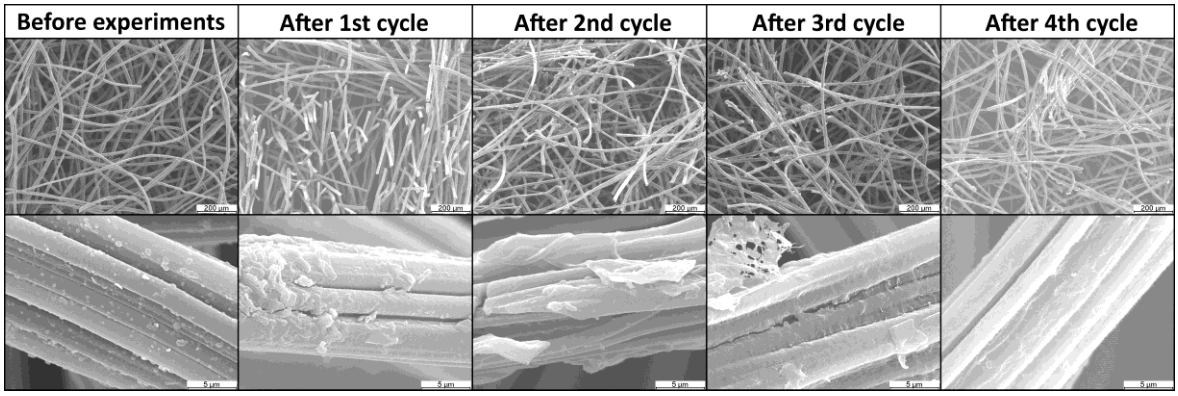

Figure 4.16 – SEM results of the analysis of the CF anode in the assays run at continuous polarity: top row - 100x amplification; bottom row - 5000x amplification.

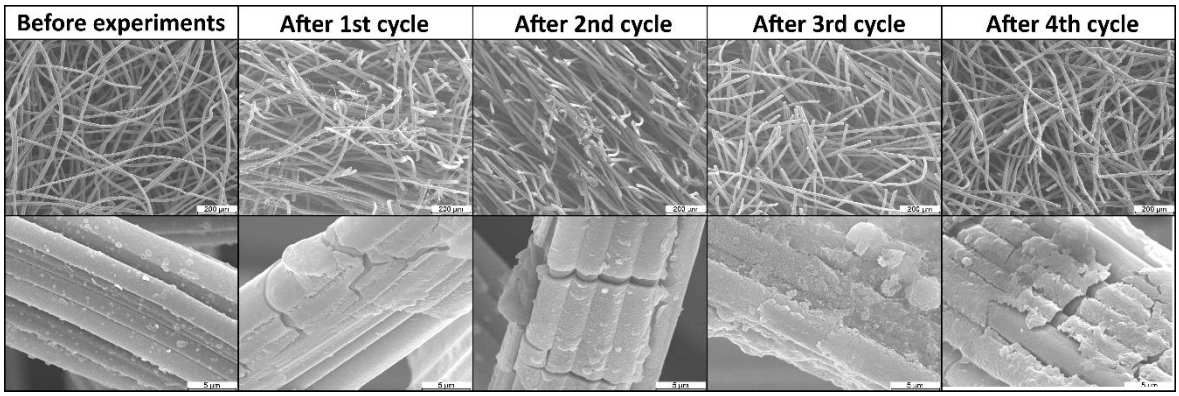

Figure 4.17 – SEM results of the analysis of the CF cathode in the assays run at continuous polarity: top row - 100x amplification; bottom row - 5000x amplification.

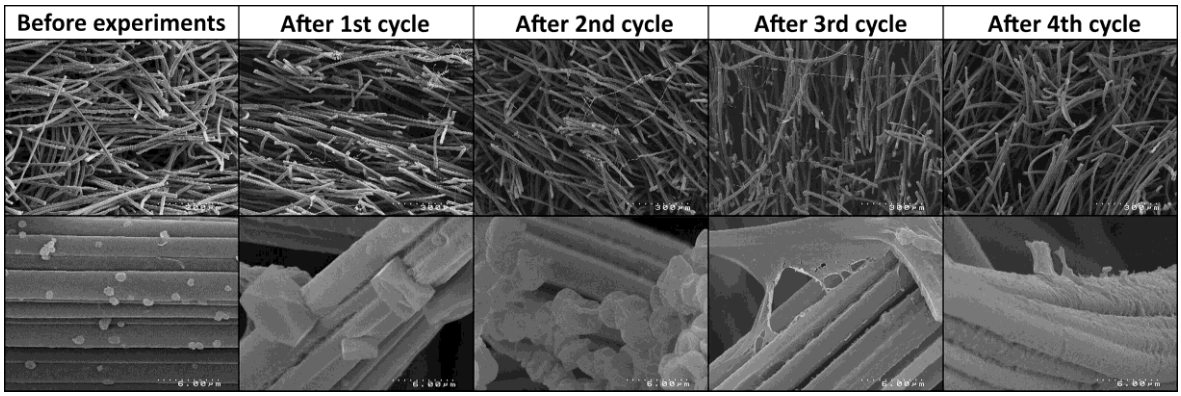

Figure 4.18 – SEM results of the analysis of the CF anode in the assays run with polarity reversal: top row - 100x amplification; bottom row - 5000x amplification.

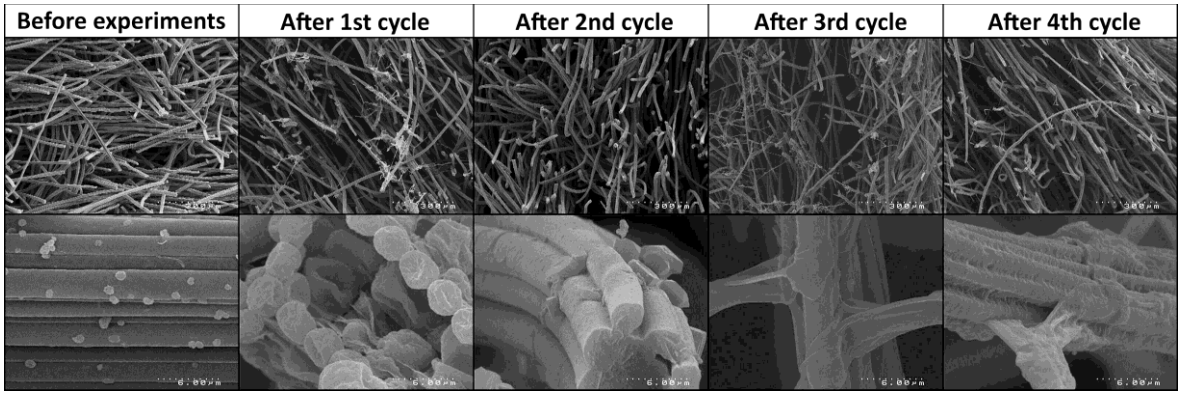

Figure 4.19 – SEM results of the analysis of the CF cathode in the assays run with polarity reversal: top row - 100x amplification; bottom row - 5000x amplification.

To further study the durability of the CF anode, consecutive assays of 24-h duration were performed, being the effluent renewed between assays. The experimental results obtained are presented in Figure 4.20.

After 60 hours, the experiment had to be stopped, since the voltage reached the limit for current control of the power source utilized. The anode didn't break during this time, like it happened in the previous experiment. It should be noticed that, at this experiment of 24-h cycle, the electrodes weren't washed, unlike it occurred at the experiment of 8-hour cycle.

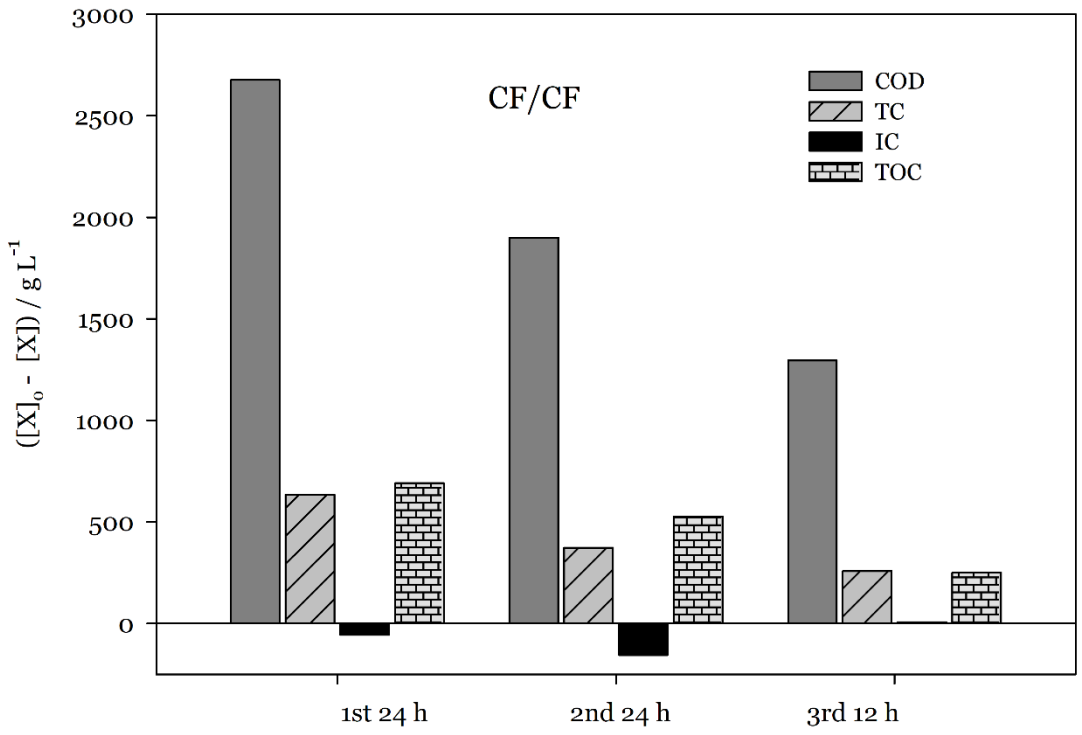

Figure 4.20 – Variation of COD, TC, IC, and TOC during each cycle.

It can be observed that, during the 60-hour assay, the removal of COD, TC, and TOC decreased along the cycles, which is probably due to the clogging of the active sites of the electrodes, as there was no washing step in this experiment.

SEM analysis of the electrodes used in the assay was carried out, with results being shown in Figures 4.21 and 4.22.

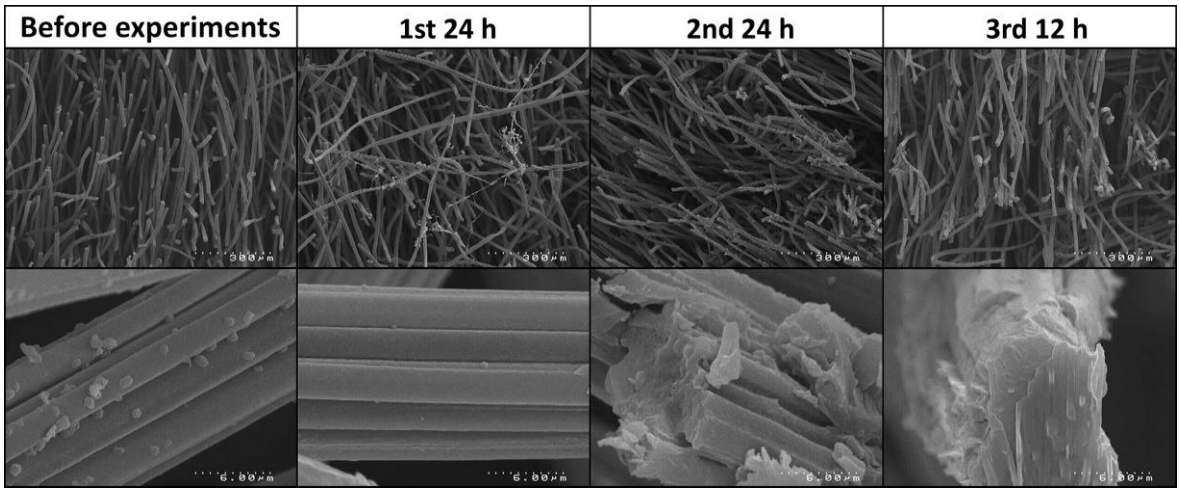

Figure 4.21 – SEM results of the analysis of the CF anode used at the consecutive assays of 24-h duration: top row - 100x amplification; bottom row - 5000x amplification.

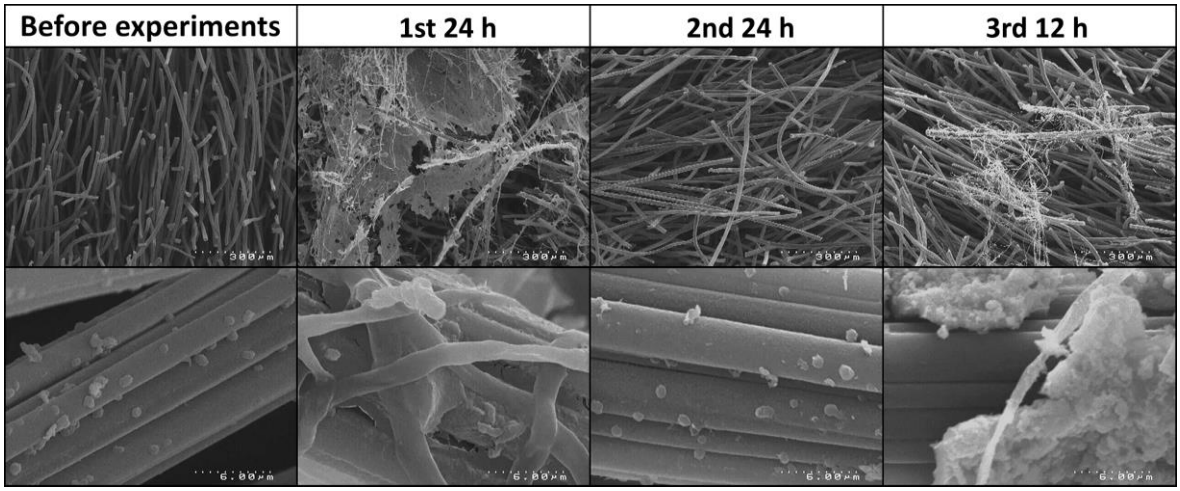

Figure 4.22 – SEM results of the analysis of the CF cathode used at the consecutive assays of 24-h duration: top row - 100x amplification; bottom row - 5000x amplification.

It can be observed that the anode sustained significant erosion, while the cathode appears to have suffered large deposition throughout the experiments. Both these factors should contribute to the decrease of the removal efficiency of the process.

While this is certainly a step back for the use of this material in electrochemical processes, it being almost inexpensive should be reason enough to further study this material.

Chapter 5 – Conclusions and future perspectives

The main goal of this work was to study the efficiency of carbon felt as electrode material in the treatment of winery wastewater through electrochemical processes, which could serve as an alternative to the existing treatment systems. To accomplish this, laboratory experiments were performed, and its results were evaluated. The conducted experiments were organized into two sections in accordance with the electrochemical process being studied. The primary conclusions for each set of experiments were reached in the "Results and discussion" chapter considering the results obtained. This chapter presents an assessment of the suggested goals based on these observations. Prior to evaluating the primary goal, secondary goals are first examined. Finally, potential application of these electrochemical processes in the treatment of winery wastewater is discussed.

The following four paragraphs, one for each of the goals put forward, analyze secondary goals.

1. Study the process efficiency of two electrochemical processes in the treatment of WW, namely electro-Fenton, and electrochemical oxidation.

This goal was accomplished, since both processes were successful in partially treating winery wastewater in the experiments set up. With up to 69% COD removal, EF process had the highest efficiency, compared with EO, which only reached up to 64% COD removal. This goes according to what has been reported in the literature.

2. Compare the results obtained with a carbon felt anode to those of a standard BDD anode.

This goal was studied throughout the EO experiments, with results showing that carbon felt demonstrates an almost similar anode capability as the BDD. In the same conditions, BDD obtained 32% COD removal whereas the CF anode obtained 28%.

3. Study other process variables and their influence in the efficiency of the process.

In the EF experiments, both applied current intensity and added Fe^{2+} concentration were variables under evaluation, with results showing that a higher current results in a higher removal rate, as does a higher initial concentration of Fe^{2+}.

The applied current intensity was again studied in the EO experiments, together with the type and concentration of electrolyte. Higher current demonstrated better results again, while the type and concentration of electrolyte didn't affect the results significantly.

4. Evaluate the durability and reproducibility of CF electrodes during these processes.

The CF electrodes proved to have good reproducibility, with results being consistent across multiple similar experiments. However, its durability didn't hold out through multiple experiments, with the electrode piece breaking apart, losing fiber density, and suffering deposition over long periods of time.

Based on the results obtained, it can be proven that the carbon felt could be an efficient electrode replacement in electrochemical processes such as electro-Fenton and electrochemical deposition, with results comparable to those of BDD, regarding load removal rate and reproducibility. However, its lack of durability still presents a major flaw and should be addressed in a future work, as a case study on how to optimize/improve it.

Regarding future works, and given the results here obtained, the use of CF electrodes in the treatment of other types of wastewaters and through other different electrochemical processes presents new possible studies to be made.

References

Anglada et al., 2009	Anglada, A., Urtiaga, A., Ortiz, I., (2009). Contributions of electrochemical oxidation to waste-water treatment: fundamentals and review of applications. J. Chem. Technol. Biotechnol. 84: 1747–1755.
Baía et al., 2022	Baía, A., Lopes, A., Nunes, M.J., Ciríaco, L., Pacheco, M.J., Fernandes, A., (2022). Removal of Recalcitrant Compounds from Winery Wastewater by Electrochemical Oxidation. Water 14: 750.
Candia-Onfray et al., 2018	Candia-Onfray, C., Espinoza, N., Silva, E.B.S., Toledo-Neira, C., Espinoza, L.C., Santander, R., García, V., Salazar, R., (2018). Treatment of winery wastewater by anodic oxidation using BDD electrode. Chemosphere 206: 709-717.
Chen et al., 2022	Chen, X., Teng, W., Fan, J., Chen, Y., Ma, Q., Xue, Y., Zhang, C., Zhang, W., (2022). Enhanced degradation of micropollutants over iron-based electro-Fenton catalyst: Cobalt as an electron modulator in mesochannels and mechanism insight. J. Hazard. Mater. 427: 127896.
Chiang et al., 1995	Chiang, L., Chang, J., Wen, T., (1995). Indirect oxidation effect in electrochemical oxidation treatment of landfill leachate. Water Res. 29 (2): 671-678.
Coetzee et al., 2017	Coetzee, R., Dorfling, C., Bradshaw, S.M., (2017). Characterization of precipitate formed during the removal of iron and precious metals from sulphate leach solutions. J. S. Afr. Inst. Min. Metall., 117 (8): 771-778.
Comninellis, 1994	Comninellis, C., (1994). Electrocatalysis in the electrochemical conversion/combustion of organic pollutants for wastewater treatment. Electrochim. Acta 39 (11/12): 1857-1862.
Davididou & Frontistis, 2021	Davididou, K., Frontistis, Z., (2021), Advanced oxidation processes for the treatment of winery wastewater: a review and future perspectives. J. Chem. Technol. Biotechnol. 96: 2436-2450.
Deng & Englehardt, 2006	Deng, Y., Englehardt, J.D., (2006). Treatment of landfill leachate by the Fenton process. Water Res. 40 (20): 3683-3694.
Díez et al., 2016	Díez, A.M., Iglesias, O., Rosales, E., Sanromán, M.A., Pazos, M., (2016). Optimization of two-chamber photo electro Fenton reactor for the treatment of winery wastewater. Process Saf. Environ. Prot. 101: 72-79.
Díez et al., 2017a	Díez, A.M., Rosales, E., Sanromán, M.A., Pazos, M., (2017). Assessment of LED-assisted electro-Fenton reactor for the treatment

of winery wastewater. J. Chem. Eng. 310 (2): 399-406.

Díez et al., 2017b — Díez, A.M., Sanromán, M.A., Pazos, M., (2017). Sequential two-column electro-Fenton-photolytic reactor for the treatment of winery wastewater. Environ. Sci. Pollut. Res. 24: 1137-1151.

Doumbi et al., 2022 — Doumbi, R.T., Noumi, G.B., Ngobtchok, B., Domga, (2022). Tannery wastewater treatment by electro-Fenton and electro-persulfate processes using graphite from used batteries as free-cost electrode materials. Case Stud. Chem. Environ. Eng. 5: 100190.

Eaton et al., 2005 — Eaton, A., Clesceri, L., Rice, E., Greenberg, A., Franson, M.A.. Standard Methods for Examination of Water and Wastewater, twenty-first ed., American Public Health Association, Washington, DC, 2005.

Elmagirbi et al., 2012 — Elmagirbi, A., Sulistyarti, H., Atikah, (2012). Study of Ascorbic Acid as Iron(III) Reducing Agent for Spectrophotometric Iron Speciation. J. Pure App. Chem. Res. 1 (1): 11-17.

Fernandes et al., 2015 — Fernandes, A., Pacheco, M.J., Ciríaco, L., Lopes, A., (2015). Review on the electrochemical processes for the treatment of sanitary landfill leachates: Present and future. Appl. Catal. B: Environ. 176-177: 183-200.

Fernandes et al., 2016 — Labiadh, L., Fernandes, A., Ciríaco, L., Pacheco, M.J., Gadri, A., Ammar, S., Lopes, A., (2016). Electrochemical treatment of concentrate from reverse osmosis of sanitary landfill leachate. J. Environ. Manage. 181: 515-521.

Fernandes et al., 2017 — Fernandes, A., Labiadh, L., Ciríaco, L., Pacheco, M.J., Gadri, A., Ammar, S., Lopes, A., (2017). Electro-Fenton oxidation of reverse osmosis concentrate from sanitary landfill leachate - Evaluation of operational parameters. Chemosphere 184: 1223-1229.

Fernandes et al., 2019 — Fernandes, A., Chamem, O., Pacheco, M.J., Ciríaco, L., Zairi, M., Lopes, A., (2019). Performance of Electrochemical Processes in the Treatment of Reverse Osmosis Concentrates of Sanitary Landfill Leachate. Molecules 24(16): 2905.

Fernandes et al., 2021 — Fernandes, A., Nunes, M.J., Rodrigues, A.S., Pacheco, M.J., Ciríaco, L., Lopes, A., (2021). Electro-Persulfate Processes for the Treatment of Complex Wastewater Matrices: Present and Future. Molecules 26(16): 4821.

Fryda et al., 1999 — Fryda, M., Herrmann, D., Schäfer, L., Klages, C., Perret, A., Haenni, W., Comninellis, C., Gandini, D., (1999). Properties of diamond electrodes for wastewater treatment. New Diam. Front. Carbon Technol. 9(3): 229-240.

Iglesias et al., 2015 — Iglesias, O., Meijide, J., Bocos, E., Sanromán, M.A., Pazos, M., (2015). New approaches on heterogeneous electro-Fenton treatment of winery. Electrochim. Acta 169: 134-141.

Ippolito et al., 2021 — Ippolito, N.M., Zueva, S.B., Ferella, F., Corradini, V., Baturina, E.V., Vegliò, F., (2021). Treatment of waste water from a winery with an advanced oxidation process (AOP). IOP Conf. Ser.: Earth Environ. Sci. 640: 062025.

ISO 6332:1988 — ISO 6332:1988. Water Quality — Determination of Iron — Spectrometric Method Using 1,10-Phenanthroline; ISO: Geneva, Switzerland, 1988.

Johnson & Mehrvar, 2020 — Johnson, M.B., Mehrvar, M., (2020). Characterising winery wastewater composition to optimise treatment and reuse. Aust. J. Grape Wine Res. 26: 410-416.

Karimi et al., 2022 — Karimi, A., Mohamadi, H., Fathifar, E., (2022). Evaluation of Textile Wastewater Treatment Using Combined Methods - Factor Optimization via Split Plot RSM. Iran. J. Chem. Chem. Eng. 41(2): 607-617

Lauzurique et al., 2022 — Lauzurique, Y., Espinoza, L.C., Huiliñir, C., García, V., Salazar, R., (2022). Anodic Oxidation of Industrial Winery Wastewater Using Different Anodes. Water 14(1): 95.

Liang et al., 2008 — Liang, C., Huang, C.-F., Mohanty, N., Kurakalva, R.M., (2008). A rapid spectrophotometric determination of persulfate anion in ISCO. Chemosphere 73: 1540–1543.

Ltaïef et al., 2019 — Ltaïef, A.H., Gadri, A., Ammar, S., Fernandes, A., Nunes, M.J., Ciríaco, L., Pacheco, M.J., Lopes, A., (2020). Olive mill wastewater treatment by electro-Fenton with heterogeneous iron source. In WASTES – Solutions, Treatments and Opportunities III, Selected Papers from the 5th International Conference Wastes: Solutions, Treatments and Opportunities, Costa da Caparica, Lisbon, Portugal, 4-6 September 2019. Edited by Vilarinho, C., Castro, F., Gonçalves, M., Fernando, A.L., CRC Press/Balkema, Leiden, The Netherlands, ISBN: 978-0-367-25777-4, 333-338.

Malakootian & Ahmadian, 2019 — Malakootian, M., Ahmadian, M., (2019). Ciprofloxacin removal by electro-activated persulfate in aqueous solution using iron electrodes. Appl. Water. Sci. 9: 140.

Martínez-Cruz et al., 2020 — Martínez-Cruz, A., Fernandes, A., Ciríaco, L., Pacheco, M.J., Carvalho, F., Afonso, A., Madeira, L., Luz, S., Lopes, A. (2020). Electrochemical Oxidation of Effluents from Food Processing Industries: A Short Review and a Case-Study. Water 12(12): 3546.

Martínez-Huitle & Brillas, 2009 — Martínez-Huitle, C.A., Brillas, E., (2009). Decontamination of wastewaters containing synthetic organic dyes by electrochemical methods - A general review. Appl. Catal. B: Environ. 87(3-4): 105-145.

Martínez-Huitle & Ferro, 2006 — Martínez-Huitle, C.A., Ferro, S., (2006). Electrochemical oxidation of organic pollutants for the wastewater - direct and indirect processes. Chem. Soc. Rev. 35: 1324-1340.

Moreira et al., 2015 — Moreira, F.C., Boaventura, R.A.R., Brillas, E., Vilar, V.J.P., (2015). Remediation of a winery wastewater combining aerobic biological oxidation and electrochemical advanced oxidation processes. Water Res. 75: 95-108.

Moreira et al., 2017 — Moreira, F.C., Boaventura, R.A.R., Brillas, E., Vilar, V.J.P., (2017). Electrochemical advanced oxidation processes - A review on their application to synthetic and real wastewaters. Appl. Catal. B: Environ. 202: 217-261.

Mosse et al., 2011 — Mosse, K.P.M., Patti, A., Christen, E., Cavagnaro, T., (2011). Review: Winery wastewater quality and treatment options in Australia. Aust. J. Grape Wine Res. 17: 111-122.

Nidheesh & Gandhimathi, 2012 — Nidheesh, P.V., Gandhimathi, R., (2012). Trends in electro-Fenton process for water and wastewater treatment - An overview. Desalination 299: 1-15.

Nogueira et al., 2005 — Nogueira, R.F.P., Oliveira, M.C., Paterlini, W.C., (2005). Simple and fast spectrophotometric determination of H_2O_2 in photo-Fenton reactions using metavanadate. Talanta 66(1): 86-91.

Orkun et al., 2012 — Orkun, M.O., Kuleyin, A., (2012). Treatment performance evaluation of chemical oxygen demand from landfill leachate by electro-coagulation and electro-fenton technique. Environ. Prog. Sustain. Energy 31: 59-67.

Panizza et al., 2001 — Panizza, M., Michaud, P.A., Cerisola, G., Comninellis, C., (2001). Anodic oxidation of 2-naphthol at boron-doped diamond electrodes. J. Electroanal. Chem. 507(1-2): 206-214.

Panizza et al., 2005 — Panizza, M., Cerisola, G., (2005). Application of diamond electrodes to electrochemical processes. Electrochim. Acta 51(2): 191-199.

Perry et al., 2019 — Perry, S.C., Pangotra, D., Vieira, L., Csepei, L., Sieber, V., Wang, L., León, C.P., Walsh, F.C., (2019). Electrochemical synthesis of hydrogen peroxide from water and oxygen. Nat. Rev. Chem. 3: 442-458.

Santos et al., 2022 — Santos, M.C., Antonin, V.S., Souza, F.M., Aveiro, L.R., Pinheiro, V.S., Gentil, T.C., Lima, T.S., Moura, J.P.C., Silva, C.R., Lucchetti, L.E.B., Codognoto, L., Robles, I., Lanza, M.R.V., (2022) Decontamination of wastewater containing contaminants of emerging concern by electrooxidation and Fenton-based processes – A review of materials and methods. Chemosphere 307(3): 135763.

Sirés et al., 2007 — Sirés, I., Garrido, J.A., Rodríguez, R.M., Brillas, E., Oturan, N., Oturan, M.A., (2007). Catalytic behavior of the Fe^{3+}/Fe^{2+} system in the electro-Fenton degradation of the antimicrobial chlorophene. Appl. Catal. B: Environ. 72(3-4): 382-394.

Sirés et al., 2014 — Sirés, I., Brillas, E., Oturan, M.A., Rodrigo, M.A., Panizza, M., (2014). Electrochemical advanced oxidation processes: today and tomorrow.

A review. Environ. Sci. Pollut. Res. 21: 8336–8367.

Solarchem Environmental Systems, 1994 — Solarchem Environmental Systems. The UV/oxidation Handbook. Solarchem Environmental Systems, Markham, Ont., Canada, 1994.

Strong & Burgess, 2008 — Strong, P.J., Burgess, J.E., (2008). Treatment Methods for Wine-Related and Distillery Wastewaters: A Review. Bioremediat. J. 12 (2): 70-87.

Umar et al., 2010 — Umar, M., Aziz, H.A., Yusoff, M.S., (2010). Trends in the use of Fenton, electro-Fenton and photo-Fenton for the treatment of landfill leachate. Waste Manage. 30(11): 2113-2121.

Wang et al., 2012 — Wang, Y., Li, X., Zhen, L., Zhang, H., Zhang, Y., Wang, C., (2012). Electro-Fenton treatment of concentrates generated in nanofiltration of biologically pretreated landfill leachate. J. Hazard. Mater. 229-230: 115-121.

Yang et al., 2022 — Yang, X., Chen, Z., Du, S., Meng, H., Ren, Z., (2022). Cu-coupled Fe/Fe_3C covered with thin carbon as stable win-win catalysts to boost electro-Fenton reaction for brewing leachate treatment. Chemosphere 293: 133532.

Yavuz et al., 2012 — Yavuz, Y., Shahbazi, R., (2012). Anodic oxidation of Reactive Black 5 dye using boron doped diamond anodes in a bipolar trickle tower reactor. Sep. Purif. Technol. 85: 130-136.

Zhang et al., 2006 — Zhang, H., Zhang, D., Zhou, J., (2006). Removal of COD from landfill leachate by electro-Fenton method. J. Hazard. Mater. 135(1-3): 106-111.

Zhang et al., 2012 — Zhang, H., Ran, X., Wu, X., (2012). Electro-Fenton treatment of mature landfill leachate in a continuous flow reactor. J. Hazard. Mater. 241-242: 259-266.

Zhang et al., 2022 — Zhang, C., Dionysiou, D.D., Li, F., Zhang, H., Fang, X., Fu, H., He, J., Chen, L., Ying, G., Huang, M., (2022). Designing NAZO@BC electrodes for enhanced elimination of hydrophilic organic pollutants in heterogeneous electro-Fenton system: Insights into the detoxification mediated by $^1O_2$ and •OH. J. Hazard. Mater. 431: 128598.